Palmitoylated Importin α Regulates Mitotic Spindle Orientation Through Interaction with NuMA

Authors

Patrick James Sutton[1,*], Natalie Mosqueda[1] and Christopher W. Brownlee[1,2]

Author Affiliations and Footnotes

[1]Department of Pharmacological Sciences, Stony Brook University; Stony Brook, 11794, United States of America.

[2]Lead Contact

*Correspondence: Patrick.Sutton@stonybrook.edu (P.J.S),

Christopher.Brownlee@stonybrook.edu (C.W.B)

Abstract

Regulation of cell division orientation is a fundamental process critical to differentiation and tissue homeostasis. Microtubules emanating from the mitotic spindle pole bind a conserved complex of proteins at the cell cortex which orients the spindle and ultimately the cell division plane. Control of spindle orientation is of particular importance in developing tissues, such as the developing brain. Misorientation of the mitotic spindle and thus subsequent division plane misalignment can contribute to improper segregation of cell fate determinants in developing neuroblasts, leading to a rare neurological disorder known as microcephaly. We demonstrate that the nuclear transport protein importin α, when palmitoylated, plays a critical role in mitotic spindle orientation through localizing factors, such as NuMA, to the cell cortex. We also observe craniofacial developmental defects in *Xenopus laevis* when importin α palmitoylation is abrogated, including smaller head and brains, a hallmark of spindle misorientation and microcephaly. These findings characterize not only a role for importin α in spindle orientation, but also a broader role for importin α palmitoylation which has significance for many cellular processes.

Introduction

Mitotic spindle orientation is a fundamental cellular process which regulates cell division orientation, a crucial aspect of mitosis that when dysregulated can lead to uncontrolled asymmetric division and overproliferation, or developmental defects due to premature stem cell differentiation, depending on the cell type (Bergstralh and St Johnston, 2014; Bergstralh et al., 2017; Charnley et al., 2013; Finegan and Bergstralh, 2019). Neuronal development in particular is heavily reliant on properly oriented cell divisions to ensure the correct timing of neuron

differentiation, a process that when disturbed can result in severe defects, such as microcephaly (Razuvaeva et al., 2023; Higgins and Goldstein, 2010; Konno et al., 2008).

Mitotic spindle orientation is largely controlled by the anchoring of astral microtubules (aMTs) to the cell cortex in metaphase, and the pulling force generated by the dynein/dynactin motor complex on aMTs during anaphase (Kiyomitsu and Cheeseman, 2012; Kotak and Gönczy, 2013; Toyoshima and Nishida, 2007; Pietro et al., 2016; Bergstralh et al., 2017; Singh et al., 2021; Yang et al., 2014; Anjur-Dietrich et al., 2024). aMTs are anchored at the cortex by a conserved complex of proteins consisting of Gαi, which through myristylation is thought to associate with the plasma membrane (PM), Leucine-Glycine-Asparagine repeat containing protein (LGN), which binds to Gαi, and Nuclear Mitotic Apparatus (NuMA), which binds to LGN and dynein/dynactin, facilitating the strong pulling force on the aMTs necessary for maintenance of spindle orientation in metaphase (Higgins and Goldstein, 2010; Pietro et al., 2016; Camuglia et al., 2022; Kiyomitsu and Cheeseman, 2012; Fankhaenel et al., 2023; He et al., 2023; Kiyomitsu and Boerner, 2021; Zheng et al., 2013; Okumura et al., 2018; Pirovano et al., 2019; Du and Macara, 2004; Neville et al., 2022; Yu et al., 2000; Bowman et al., 2006; Carvalho et al., 2015; Anjur-Dietrich et al., 2024). While all of these factors play a role in aMT anchoring during metaphase, only NuMA and dynein/dynactin are required during anaphase to ensure the proper separation of chromatin to the poles (Bergstralh and St Johnston, 2014; Kotak et al., 2014; Seldin et al., 2013). Additionally, it has been shown that LGN and Gαi are only required for NuMA localization to the cell cortex during metaphase, not anaphase (Okumura et al., 2018; Kiyomitsu and Boerner, 2021). However, it remains unclear how these factors localize to the PM during metaphase and how this membrane localization is maintained there when it is believed that only a singly myristoylated Gαi is responsible for membrane association of the entire aMT

anchoring complex. Recently it has been demonstrated that a single dynein motor interacts with each aMT, suggesting that only a single complex of Gai, LGN, NuMA, and dynein is present at the cortex for each aMT. This highlights the need for this complex to be strongly associated with the PM (Anjur-Dietrich et al., 2024). Furthermore, the necessity for a significant pulling force towards the PM during metaphase to orient the mitotic spindle and during anaphase to facilitate separation of chromatin to the poles suggests that an additional factor, which can associate with the PM via multiple interaction points, may be involved in aMT anchoring.

Importin α is a highly conserved and abundant protein known for functioning as a nuclear transport adapter in interphase and as a spindle assembly factor during mitosis through its ability to bind Nuclear Localization Signal (NLS) sequence containing proteins (Takeda et al., 2011; Oka and Yoneda, 2018; Goldfarb et al., 2004). However in recent years, a number of proteomic screens for palmitoylated proteins utilizing a variety of biochemical methods and mass spectrometry verification have identified human importin α-1 (KPNA2) as a target for palmitoylation (Won and Martin, 2018; Thinon et al., 2018; Serwa et al., 2015; Mariscal et al., 2020; Schelar and Liu, 2008; Zhou et al., 2019; Sobocinska et al., 2018). Palmitoylation is a reversible and dynamic process which modifies proteins post translationally with palmitate lipids allowing both diffusion and vesicle mediated transport of palmitoylated proteins to the PM (Guan and Fierke, 2011). Additionally, recent work in *Xenopus laevis* (*X. laevis*) revealed that importin α can be reversibly sequestered to the PM via palmitoylation of 4 key residues, 3 of which are conserved in humans (Brownlee and Heald, 2019). This same study found that when palmitoylated, importin α acts as an evolutionarily conserved cell-surface area-to-volume sensor that coordinately scales nuclear and spindle size to cell size. Following this work, mass spectrometry methods have confirmed palmitoylation of at least one residue in human KPNA2 in

addition to the 3 residues conserved from *X. laevis* importin α-1 (Zhou et al., 2019) and palmitoylation prediction screens have identified additional cysteine residues in human KPNA2 likely to be palmitoylated with high confidence. These findings raise the intriguing possibility that importin α may have roles other than as a nuclear import adapter upon palmitoylation (Brownlee and Heald, 2019).

Due to the requirement of an exceedingly strong pulling force to drive orientation of the spindle and chromatin separation to the poles, we hypothesize that palmitoylated importin α could provide a sufficiently strong interaction with the PM to anchor aMTs in mitosis. Importin α when modified with palmitate lipids at multiple residues would provide a significantly increased membrane association compared to singly myristoylated Gαi and could increase the membrane association of the aMT anchoring complex as a whole if bound to the factors involved. Notably, NuMA as well as Discs Large (Dlg), another protein recently implicated in spindle orientation (Bergstralh et al., 2016; Carvalho et al., 2015; Saadaoui et al., 2014; Schiller and Bergstralh, 2021), contain strongly predicted NLS sequences suggesting importin α may be responsible for their cellular localization through importin α-NLS binding. Previous literature has also investigated the effects of deleting the NLS of NuMA and determined that NuMA's NLS is required for its cortical localization (Okumura et al., 2018). Additionally, findings which demonstrate that NuMA does not require LGN or Gαi to localize to the polar cortex during late anaphase raise the intriguing possibility that palmitoylated importin α may play a role in NuMA's mitotic localization (Okumura et al., 2018; Kiyomitsu and Boerner, 2021). We hypothesize that palmitoylated importin α could bind NuMA's NLS in metaphase, transport it to the PM and therefore be necessary for NuMA's localization in metaphase and early anaphase, and sufficient for NuMA's localization during late anaphase.

A key factor driving protein localization and spindle formation in mitosis is a gradient of RanGTP generated by the chromosome-tethered RanGEF, RCC1 (Kalab and Heald, 2008). In interphase, the same localized concentration of RanGTP in the nucleus facilitates release of cargo from importins for proper nuclear transport (Kalab and Heald, 2008; Ozugergin and Piekny, 2021). All of these processes are driven by the binding of RanGTP to importin β, which causes the dissociation of importins and any bound cargo (Kalab and Heald, 2008; Oka and Yoneda, 2018). In mitosis, chromosomes are arranged during metaphase in such a manner that the tethered RCC1 generates a high concentration of RanGTP at the midline of the cell, but a low concentration of RanGTP towards the poles (Ems-McClung et al., 2020). The lack of RanGTP at the polar cortex and the abundance of RanGTP at the lateral cortex during metaphase due to the equatorial localization of the mitotic Ran gradient indicates that importin α can remain bound to NLS containing cargo at the polar cortex exclusively. Importantly, this is where aMTs are anchored and NuMA has been found to localize (Kiyomitsu and Cheeseman, 2012; Oka and Yoneda, 2018; Chang et al., 2017; Kalab and Heald, 2008; Ems-McClung et al., 2020). This suggests that the Ran gradient can regulate the localization of NLS containing proteins at the PM and therefore restrict localization of NuMA to the polar cortex, through interaction with palmitoylated importin α. Additionally, it has been shown that manipulation of the Ran gradient disrupts spindle orientation and the localization of spindle orientation factors (Kiyomitsu and Cheeseman, 2013).

In the present work we demonstrate that importin α when palmitoylated is a key regulator of mitotic spindle orientation through localization of NuMA to the PM during metaphase and as such palmitoylation of importin α is required for proper control of cell division orientation. We show that palmitoylated importin α can localize throughout the PM in mitotic cells and that

palmitoylation of importin α is required for both proper spindle orientation and proper NuMA localization in metaphase. While importin α localizes to the entire PM when palmitoylated (at both the lateral and polar cortex), the accumulation of RanGTP near the metaphase plate would preclude importin α binding to NuMA, leading to accumulation of NuMA specifically to the polar cortex, where aMTs are anchored. We also explore the effects of importin α palmitoylation disruption on neuronal development in *X. laevis* and observe microcephaly which can be rescued upon forcing importin α to the PM independent of palmitoylation, further supporting that PM localization of palmitoylated importin α is a key regulator of mitotic spindle orientation.

Results

Importin α Localizes to The Mitotic Polar Cortex at Metaphase in a Palmitoylation-Dependent, but Not Cargo-Dependent Manner

Importin α has long been recognized for its role in spindle assembly during mitosis by facilitating the transport of spindle assembly factors to the midline of the cell, where mitotic spindles form (Kalab and Heald, 2008; Kaláb et al., 2006; Weaver and Walczak, 2015; Goldfarb et al., 2004). Furthermore, it has been demonstrated to influence spindle orientation through regulation of TPX2 activity (Guo et al., 2019). However, recent work has demonstrated in *X. laevis* that importin α can be post translationally modified with palmitate lipids to drive PM localization (Brownlee and Heald, 2019). These palmitoylation sites are conserved in human importin α and additional palmitoylation sites have been confirmed by palmitoylation prediction screens (Figure EV1A) and multiple mass spectrometry studies of global palmitoylated proteins (Mariscal et al., 2020; Zhou et al., 2019; Won and Martin, 2018; Thinon et al., 2018; Serwa et al., 2015; Sobocinska et al., 2018). Additionally, NLS prediction screens have shown an enrichment

of NLS containing proteins which localize to the PM and play a role in a variety of cellular processes, including spindle orientation (Figure EV1B&C).This suggests that palmitoylated importin α may be involved in mitotic cellular processes outside of spindle assembly at the PM by binding NLS containing proteins and localizing them there.

We sought to investigate other possible roles of palmitoylated importin α in mitosis by either increasing or decreasing levels of palmitoylated importin α, as well as inhibiting importin α's ability to bind or release cargo. To manipulate palmitoylation of importin α, we targeted the specific proteins responsible for palmitoylating and depalmitoylating importin α. Palmitoylation is catalyzed by palmitoyl acyl transferases (PATs), which attach palmitoyl groups to serine or cysteine residues, while depalmitoylation is carried out by acyl protein thioesterases (APTs) which remove palmityl groups (Guan and Fierke, 2011). To modulate palmitoylation levels specifically, we used small molecule inhibitors to target porcupine (PORCN), the serine PAT responsible for palmitoylation of serine residues on importin α, and APT1, the APT responsible for depalmitoylation of importin α (Brownlee and Heald, 2019). HCT116 colorectal cancer cells were selected for this study due to their established role as a model system for both spindle orientation and NuMA localization (Okumura et al., 2018; Tsuchiya et al., 2021).

We investigated the role of importin α in palmitoylation-mediated PM targeting using HCT116 cells synchronized in metaphase and treated with either DMSO (control) or Wnt-C59, a competitive inhibitor of PORCN (Proffitt et al., 2013). Wnt-C59 treatment would be expected to result in a reduction in cellular palmitoylated importin α levels, leading to a decrease in the population of importin α localized to the PM. Conversely, palmostatin treatment, which inhibits APT1 (Dekker et al., 2010; Lin and Conibear, 2015), would be expected to result in an increase

in palmitoylated importin α levels, known as hyper-palmitoylation, which would increase the population of importin α localized to the PM.

Mitotic importin α cellular localization was assessed after 1 hour in the respective drug treatments, with cell boundaries determined by bright-field microscopy (Figure EV2A). In DMSO control cells, importin α is observed localizing to centrosomes, near the assembling spindles, and at the PM (Figure 1A). Notably, Wnt-C59 treatment resulted in a 6-fold decrease of importin α signal at the PM and a concurrent enrichment of importin α signal in the cytoplasm (Figure 1A-D), while palmostatin treatment did not alter importin α PM localization compared to DMSO control treatment (Figure 1A-D). PM localization in DMSO control cells was confirmed by western blot analysis of subcellular-fractioned HCT116 cells. HCT116 cells were metaphase arrested and fractionated into 4 fractions: nuclear, cytoplasmic, organelles, and PM. The PM and cytoplasmic fractions were analyzed by SDS-PAGE and immunoblotted for β-tubulin, as a cytoplasmic marker, plasma membrane Ca^{2+} ATPase1 (PMCA1), as a PM marker, and importin α. β-tubulin was detected only in the cytoplasmic fraction and PMCA1 was detected only in the PM fraction demonstrating proper isolation of cellular fractions. However, importin α was detected in both the cytoplasmic and PM fractions confirming our immunofluorescence findings that importin α localizes to the PM in metaphase-arrested cells (Figure 1E). These results collectively suggest that palmitoylation of importin α during metaphase is required for its proper localization to the cortex.

The localization of importin α during metaphase was also analyzed in the presence of drugs that disrupt its ability to bind and release cargo. Metaphase-arrested HCT116 cells were treated with either ivermectin, a small molecule inhibitor that prevents the binding of importin α to NLS containing cargoes (Wagstaff et al., 2012) or importazole, a small molecule inhibitor of

importin based nuclear transport that prevents RanGTP mediated release of cargo from importins (Soderholm et al., 2011) (Figure 1A-D). We observed that in both importazole and ivermectin treated cells, importin α remained unperturbed at the PM (Figure 1A-D). Notably, in all drug treatments mitotic spindles were still formed properly despite disruption of importin α palmitoylation or NLS cargo binding. Taken together, these results suggest importin α partitions to the mitotic cortex via palmitoylation and does not require binding of NLS-containing cargoes to localize to the PM.

It is noteworthy that we also observe alterations in chromatin size in metaphase cells treated with our drug array. Specifically, palmostatin, importazole and ivermectin treatments appear to induce larger, more condensed chromatin compared to that observed in DMSO or Wnt-C59 treated cells. This is in line with what has previously been reported by Brownlee and Heald in 2019 and Zhou et al. in 2023. Specifically, palmitoylated importin α has been shown to regulate organelle size scaling (Brownlee and Heald, 2019) and chromatin size scaling (Zhou et al., 2023).

Importin α Palmitoylation and Cargo Binding Is Required for Proper Mitotic Spindle Orientation

We next sought to determine the effect of both disrupting importin α's ability to properly bind NLS-containing cargo and importin α mislocalization on the orientation of the metaphase mitotic spindle. HCT116 cells were metaphase-arrested and treated with DMSO, Wnt-C59, palmostatin, importazole, ivermectin, or 2-bromopalmitate, a pan palmitoylation inhibitor (Lin and Conibear, 2015). The angle of the metaphase spindle was then calculated using the relative horizontal and vertical distances between the two spindle poles (Figure 1F). Mitotic spindles were found to be misoriented in all treatments other than palmostatin relative to the DMSO-

treated control (Figure 1G & H). Interestingly, disruption of importin α palmitoylation (Wnt-C59 treatment), which was previously shown to alter mitotic importin α localization, and disruption of importin α's ability to properly bind and release cargo (ivermectin and importazole treatments respectively) both resulted in spindle misorientation. These data suggest that importin α palmitoylation is required for proper spindle orientation, and spindle orientation is dependent upon importin α binding of NLS-containing cargo.

To determine if the spindle misorientation phenotypes observed when HCT116 cells were treated with palmitoylation disrupting drugs were specifically due to mislocalization of importin α from the cell cortex, we constructed a plasmid containing importin α modified with a C-terminal CaaX domain. Addition of the CaaX domain to importin α facilitates its cortical localization through farnesylation, irrespective of its palmitoylation status (Figure EV3). Unlike palmitoylation, farnesylation is irreversible, enabling CaaX-modified proteins to be directed to the membrane and remain tethered there(Tang et al., 2009; Tamanoi et al., 2001). HCT116 cells were transfected via nucleofection to express CaaX-modified importin α or an unmodified importin α 24 hours prior to metaphase arrest and subsequent drug treatment with DMSO or Wnt-C59. We observed that HCT116 cells overexpressing unmodified importin α exhibited significantly misoriented spindle structures when treated with Wnt-C59 compared to DMSO treatment (Figure 1J). However, HCT116 cells overexpressing CaaX-modified importin α did not exhibit misorientation of spindle structures under the same conditions (Figure 1I and J), therefore rescuing spindle misorientation in Wnt-C59 treatment. This suggests that the spindle misorientation phenotypes observed when palmitoylation is disrupted are specifically due to mislocalization of importin α to the mitotic cell cortex.

Several cancer cell lines have been shown to harbor various mutations which exacerbate mitotic spindle orientation phenotypes (Chhabra and Booth, 2021). Therefore, we repeated the previous spindle orientation experiment using an hTERT immortalized cell line, RPE-1, treated with Wnt-C59 and palmostatin (Figure 1K). We again observed that Wnt-C59, but not palmostatin treatment resulted in mitotic cells with significantly misoriented spindle structures relative to the DMSO control (Figure 1L). This confirmed the findings in HCT116 cells and further suggests that palmitoylation of importin α is required for proper mitotic spindle orientation.

Previous research has indicated that cell shape and stretch play a role in determining the axis of spindle orientation and, consequently, division orientation (Finegan and Bergstralh, 2019; Charnley et al., 2013). While recent work has demonstrated that mechanical force applied to cells through stretching has a more pronounced effect on spindle orientation (by directly influencing NuMA localization) than cell shape (Tarannum et al., 2022), we sought to determine whether our palmitoylation and importin function-disrupting drug array had an impact on mitotic cell shape. We measured the circularity of 60 mitotic HCT 116 cells per drug treatment and observed that there was no significant reduction in cell circularity in any of our drug treatments (Figure EV2B). In fact, palmostatin-treated cells exhibited a slightly increased circularity compared to DMSO treated cells (Figure EV2B). These findings confirm that the observed spindle misorientation is not attributable to alterations in cell shape.

Importin α Interacts with NuMA but not Dlg at the Metaphase Cell Cortex

Mitotic spindle orientation in vertebrates is mediated through aMT anchoring at the cell cortex via a conserved protein complex consisting of LGN, Gαi, NuMA and dynein/dynactin (Bergstralh et al., 2017). Of these known spindle orientation proteins, only NuMA contains a

known NLS sequence, suggesting it may be a potential binding partner of importin α. To confirm the interaction between importin α and NuMA, we performed immunoprecipitation of the endogenous proteins from metaphase-arrested HCT116 cells treated with DMSO, Wnt-C59 and palmostatin. Our results demonstrated that importin α and NuMA coprecipitated equally in all drug treatment conditions (Figure 2A), confirming importin α and NuMA binding which is unaffected by palmitoylation disruption.

To further investigate if importin α-NuMA interactions occur specifically at the mitotic cortex, where aMTs are anchored, we employed a rolling amplification based proximity ligation assay (PLA) (Alam, 2018). Additionally, we also probed for importin a-Dlg interactions at the mitotic cortex using the same assay, as Dlg has been recently implicated in spindle orientation (Schiller and Bergstralh, 2021; Saadaoui et al., 2014; Bergstralh et al., 2016), and contains a predicted NLS sequence. Therefore, we also probed for importin α-Dlg interactions at the mitotic cortex using the same assay. Importin α interaction with NuMA or Dlg was quantified by measuring the number of PLA foci in 3 regions of interest at the polar cortex, lateral cortex, and in the cytoplasm to determine where in the cell these proteins were interacting (Figure 2B). PLA was performed on metaphase-arrested HCT116 cells in DMSO control, Wnt-C59 and palmostatin treated conditions using specific antibodies to importin α and either NuMA or Dlg (Figure 2C and E, respectively). The assay revealed that importin α and NuMA interact at the polar cortex of DMSO treated metaphase cells, but not Wnt-C59 treated cells. Additionally, importin α-NuMA interactions were found at both the polar and lateral cortices in palmostatin treated cells (Figure 2D). Palmostatin treated cells also exhibited a marked enrichment of importin α-NuMA interactions at the centrosomes and along spindle structures (Figure 2D) suggesting that importin α could associate more strongly with NuMA when hyper-palmitoylated.

It is noteworthy that importin α and NuMA were only found to interact at the polar cortex in control conditions as we have previously demonstrated that palmitoylated importin α localizes throughout the mitotic PM at both the polar and lateral cortex (Figure 1A). This is to be expected, as although importin α is present throughout the cortex, the presence of the RanGTP gradient at the midline of the cell prevents importin α from binding or remaining bound to the NLS of NuMA at the lateral cortex, limiting their interaction to the polar cortex where aMTs are anchored.

When probing for importin α interaction with Dlg, we observed that while importin α and Dlg were found to interact throughout the cytosol, this interaction was not enriched at any specific cellular location and was not altered by Wnt-C59 or palmostatin treatment (Figure 2F). These results collectively suggest that precise importin α palmitoylation levels are required to maintain the importin α-NuMA interaction at the mitotic polar cortex and that importin α and Dlg do not interact at the PM. A potential explanation for importin α interacting with NuMA specifically and not Dlg is that these proteins contain distinct NLS sequences, such that NuMA has a bipartite NLS while Dlg is predicted to have a monopartite NLS (Chang et al., 2017). It is plausible that palmitoylated importin α, which would need to bind to these proteins in order to localize them to the membrane, binds preferentially to some NLS containing cargo over others.

To further validate that the interaction between NuMA and importin α occurs at the polar cortex in a palmitoylation dependent manner, we transfected HCT116 cells with either importin α-mCherry-HA or importin α-mCherry-HA-CaaX. As before, we treated the cells with Wnt-C59, arrested them in metaphase, and performed a PLA for NuMA and the transfected construct (Figure 2G). We observed that cells transfected with the wild-type importin α construct treated with Wnt-C59 (Figure 2H) exhibited a PLA foci distribution similar to endogenous importin a

expressing cells treated with Wnt-C59 (Figure 2C). Conversely, cells transfected with the importin α-CaaX construct treated with Wnt-C59 displayed a PLA foci distribution more similar to DMSO-treated cells, with a significant shift in foci from the cytoplasm to the polar cortex compared to the wild-type transfected cells. This shift suggests a rescue of importin α-NuMA interactions solely by forcing importin α to the PM (Figure 2H).

To account for potential differences in NuMA or importin α protein levels after drug treatments, we performed a western blot and found that none of the treatments altered protein levels in metaphase-arrested HCT116 cells (Figure 2I, J & K). Taken together, these results suggest that importin α interacts with NuMA at the mitotic polar cortex in a palmitoylation-dependent manner.

NuMA and Dynein/Dynactin Localization During Metaphase is Dependent on NuMA Binding to Palmitoylated Importin α

It has previously been shown that deletion of NuMA's NLS causes mislocalization of NuMA away from the polar cortex (Okumura et al., 2018). Based on this and our findings that importin α palmitoylation is required for proper spindle orientation, we reasoned that importin α may be driving NuMA's mitotic localization to the polar cortex through binding NuMA's NLS and anchoring it to the PM. We therefore sought to determine how disruption of importin α palmitoylation and its ability to properly bind and release cargo could affect NuMA's mitotic localization.

Metaphase-arrested HCT116 cells expressing mClover-NuMA were treated with palmitoylation and importin α cargo binding altering drugs and analyzed for NuMA localization in metaphase (Figure 3A). NuMA intensity was measured at three cellular locations (polar cortex, lateral cortex, and cytoplasm). To account for cell-to-cell differences in fluorescent

intensity these measurements were normalized by calculating the ratio of polar cortex/lateral cortex, polar cortex/cytoplasm, and lateral cortex/cytoplasm fluorescent intensities. In the DMSO control there is an enrichment of NuMA at the polar cortex over the lateral cortex which is consistent with previously reported NuMA localization demonstrating that mClover-NuMA expression has no impact on localization (Kiyomitsu and Boerner, 2021). It is worth noting that while importin α localizes to the PM at both the lateral and polar cortices (Figure 1A), NuMA only localizes to the polar cortex in control conditions (Figure 3A). This is expected as the RanGTP gradient at the midline of the cell would prevent NLS containing cargo, such as NuMA, from remaining bound to importin α at the lateral cortex. Strikingly, NuMA polar cortex enrichment was lost in all drug conditions (Figure 3B). In Wnt-C59 and ivermectin treated cells, NuMA localization shifts away from the polar cortex and is instead enriched in the cytoplasm compared to the DMSO control (Figure 3C). In palmostatin and importazole treated cells, NuMA localization was no longer enriched at the polar cortex, but rather localized throughout the cortical membrane, including the lateral cortex (Figure 3D). This unexpected lateral cortex localization when importin α is hyper-palmitoylated upon palmostatin treatment, or cannot release cargo upon importazole treatment, suggests that importin α may be an upstream regulator of proper NuMA localization at the polar cortex. The observed NuMA localization in palmostatin-treated cells is of particular interest, as there was no significant spindle misorientation observed under these conditions, yet NuMA mislocalizes nonetheless. We hypothesize that the complete absence of NuMA at the cell cortex as observed in Wnt-C59 treated cells has a more pronounced effect on spindle misorientation than NuMA localizing to both polar and lateral cortices, as seen in palmostatin-treated cells (Figure 3A). In the conditions with no cortical NuMA, aMTs would not be anchored to the cell cortex at all, while in conditions

with NuMA present at both the polar and lateral cortices, aMTs would still anchor to the cortex albeit without spatial regulation. These results of NuMA mislocalization upon palmitoylation and importin α function disruption suggest that palmitoylated importin α membrane localization and cargo binding is necessary for NuMA's localization and maintenance to the mitotic polar cortex.

As dynein/dynactin are known to associate with the aMT anchoring complex through NuMA binding, and we have found that palmitoylated importin α is required for NuMA PM localization, we investigated the impact of disrupting importin α palmitoylation on dynactin localization in metaphase-arrested HCT116 cells. Metaphase-arrested cells were treated with DMSO, Wnt-C59 or palmostatin as described previously. We visualized $p150^{Glued}$, the large subunit of dynactin to analyze localization of dynein/dynactin (Figure 3E). Dynactin localization was quantified using the same method employed for NuMA localization. We found that in DMSO-treated control cells dynactin was enriched at the polar cortex relative to the lateral cortex and was substantially localized to the cortex relative to the cytoplasm (Figure 3F-H). This localization pattern closely resembles that of NuMA and was similarly disrupted by both Wnt-C59 and palmostatin treatments, albeit in distinct manners. In Wnt-C59 treated cells, dynactin exhibited a significant increase in the cytoplasm relative to the polar cortex (Figure 3G). Conversely, in palmostatin-treated cells, dynactin showed a significant increase at the lateral cortex relative to the polar cortex (Figure 3F). This pattern of mislocalization largely aligns with that of NuMA, suggesting that palmitoylated importin α is driving NuMA-dynein/dynactin localization to the polar cortex, facilitating aMT anchoring. Notably, unlike NuMA, dynactin did not exhibit a significant enrichment at the lateral cortex relative to the cytoplasm in palmostatin-treated cells (Figure 3H). This disparity in localization patterns could be attributed to various factors that would preclude excess dynein/dynactin from accumulating at the lateral cortex,

where the number of aMTs is significantly lower compared to the polar cortex. Further investigation is warranted to elucidate the underlying mechanisms responsible for this disparity. Nevertheless, the overall pattern of misorientation when importin α palmitoylation is disrupted strongly supports the role of palmitoylated importin α role in NuMA-dynein/dynactin localization.

Disruption of Importin α Palmitoylation Results in Microcephaly-Associated Phenotypes in *X. laevis*

Having established the role of palmitoylated importin α in mitotic spindle orientation by localizing NuMA to the polar cortex and maintaining it there, we subsequently sought to validate these findings in vivo. Numerous centrosomal and mitotic spindle orientation defects have been linked to microcephaly, as the resulting misorientation of cell division during brain development leads to a depletion of neuroprogenitor cells, and consequently, total brain tissue at the completion of development (Bergstralh and St Johnston, 2014). The African clawed frog *Xenopus laevis* has been used extensively as a model system to study microcephaly and developmental craniofacial abnormalities (Kennedy and Dickinson, 2014; Lasser et al., 2019; Shantanam and MUELLER, 2018). *X. laevis* has also been heavily utilized in mitotic spindle orientation studies exploring the roles of cell shape and stretch on NuMA localization and in turn spindle orientation (Tarannum et al., 2022; Stooke-Vaughan et al., 2017) making it an ideal system for the present study. Consequently, we utilized this model organism to determine whether mislocalization of importin α at the PM and subsequent spindle misorientation might lead to microcephaly or microcephaly-associated phenotypes. Leveraging our in vitro observations, we analyzed the effects of disrupting mitotic spindle orientation by abrogating importin α palmitoylation in the developing *X. laevis* model system.

401 *X. laevis* eggs were fertilized, placed in drug baths containing DMSO, Wnt-C59 or
402 palmostatin at approximately NF stage 24 and allowed to develop until NF stage 42 when
403 craniofacial measures can first be made (Figure 4A) (Kennedy and Dickinson, 2014; Shantanam
404 and MUELLER, 2018). Drug treated *X. laevis* embryos were assessed for craniofacial defects by
405 three metrics: distance between eyes, snout length and overall head area. Embryos were
406 immobilized in MS-222 and imaged from a dorsal perspective allowing for direct measurement
407 of cranial morphometrics. Both Wnt-C59 and palmostatin treatments significantly altered all
408 three metrics of head shape/size (Figure 4B) indicating that precise importin α palmitoylation is
409 required for proper craniofacial development in *X. laevis*. In addition to alterations in head shape,
410 drug treated tadpoles also exhibited other body morphology defects. Notably, Wnt-C59 treated
411 tadpoles exhibited much smaller tails than other conditions and a much higher mortality rate than
412 other conditions (Figure EV4).

413 While craniofacial abnormalities are a hallmark of microcephaly, we wanted to directly
414 measure potential microcephaly-associated phenotypes. We therefore sought to quantify the
415 neuroprogenitor population in the various drug treated *X. laevis* tadpoles. DMSO, Wnt-C59 and
416 palmostatin treated *X. laevis* embryos were analyzed at NF stage 46, when brain development
417 expansion reaches its apex (Exner and Willsey, 2021) by immunostaining for nestin, a
418 neuroprogenitor marker (Suzuki et al., 2010). Immunofluorescence images were taken of tadpole
419 forebrains and analyzed for the number of total cells, determined by DNA signal, that were
420 positive for nestin, indicating a neuroprogenitor identity (Figure 4C). Due to higher mortality
421 rate in Wnt-C59 treated *X. laevis* embryos, no Wnt-C59 treated tadpoles survived to NF stage 46
422 to be analyzed, indicative of severe developmental defects in both the brain and other tissue.
423 Palmostatin treated *X. laevis* embryos survived to NF stage 46 at the same rate as DMSO

controls but exhibited a significantly diminished neuroprogenitor population (Figure 4D). While total cell count remained the same from DMSO to palmostatin treatments, the number of nestin positive cells decreased (Figure 4D). This decrease in neuroprogenitors at NF stage 46 suggests that the morphometric defects observed previously are indicative of true microcephaly, which is characterized by defects in neuroprogenitor population maintenance.

To further characterize the observed microcephaly-associated phenotypes NF stage 42 drug treated *X. laevis* embryos were analyzed for the number of phosphohistone 3 (PH3) positive cells, a marker for actively dividing cells (Elmaci et al., 2018), in the brain as a decrease in active divisions of cells in the brain throughout development is a hallmark of microcephaly. Embryos treated with DMSO or Wnt-C59 were wholemount immunostained for DNA and PH3 and imaged via confocal microscopy to determine the number of cells positive for PH3 in the brain (Figure 5A). Wnt-C59 treated embryos exhibited a 6-fold decrease in the number of actively dividing cells compared to DMSO control conditions (Figure 5D). Additionally, Wnt-C59 treated embryos at NF stage 42 displayed deformed brains which lacked mid and forebrain patterning. These results together with our morphometric measurements indicate that dysregulation of palmitoylation causes craniofacial defects and particularly microcephaly in developing *X. laevis* embryos.

Forcing Importin α to the PM Rescues *X. laevis* Microcephaly Phenotypes Observed When Palmitoylation is Disrupted

Up to this point we have exclusively altered importin α palmitoylation using small molecule inhibitors, such as Wnt-C59 and palmostatin. Wnt-C59, however, exhibits off-target effects by inhibiting the PAT PORCN, which palmitoylates Wnt for secretion in addition to importin α. Given the crucial role of Wnt signaling in stemness and whole body development in

447 *X. laevis* (Yu et al., 2024), it is plausible that the observed effects in Wnt-C59-treated embryos
448 are off-target effects and cannot be directly attributed to importin α palmitoylation. Critically, to
449 address these off-target effects we investigated whether the loss of mitotic cells in the brain
450 leading to microcephaly was specifically caused by inhibiting importin α palmitoylation. To this
451 end, we utilized CaaX-modified importin α to force it to the cell membrane independently of
452 palmitoylation. Previously, we demonstrated that expression of CaaX-modified importin α could
453 rescue spindle misorientation phenotypes induced by Wnt-C59 treatment in human cell culture
454 (Figure 1E). By forcing importin α to the cell membrane while importin α palmitoylation is
455 abrogated, we can determine whether the microcephaly phenotype observed in Wnt-C59-treated
456 *X. laevis* embryos is specifically attributable to the absence of membrane-bound importin α or
457 other off-target effects.

458 We found that when *X. laevis* embryos were injected with CMV promoter-driven
459 wildtype and CaaX importin α they exhibited increased mortality and developmental defects
460 likely due to overexpression associated issues (Figure EV5). To combat this, an importin α-CaaX
461 construct was developed in a tetracycline inducible vector, pcDNA4TO, that would allow for
462 titratable levels of importin α expression. Additionally, we mitigated global developmental
463 defects of importin α overexpression by targeting expression exclusively to the D11 blastomere
464 of the developing embryo which is fated to give rise to the brain (Moody, 1987a; b*). X. laevis*
465 embryos were co-injected with importin α-CaaX pcDNA4TO and a plasmid expressing the tet
466 repressor at the D11 blastomere and analyzed for potential rescue of microcephaly (Figure 5B).

467 Importantly, *X. laevis* embryos microinjected with importin α-CaaX pcDNA4TO at the
468 D11 blastomere and treated with Wnt-C59 exhibited a rescue of PH3 levels in the brain at NF
469 stage 42 compared to uninjected Wnt-C59 treated embryos (Figure 5D). Additionally, the

microinjected tadpoles exhibited brain morphology more similar to the canonical brain morphology at this stage, as seen in the DMSO control, than compared with the uninjected Wnt-C59 treated embryos (Figure 5A&B). When treated with Wnt-C59, Importin α-CaaX injected embryos showed brain PH3 levels about 2.5 times higher than both uninjected embryos and embryos injected at D11 with an mCherry tagged CaaX domain (Figure 5C&D). Taken together, these results suggest that disrupting importin α palmitoylation leads to a loss of dividing cells in the developing *X. laevis* brain, which subsequently causes microcephaly. Furthermore, the expression of the membrane-bound importin α CaaX construct, but not the uninjected, or mCherry CaaX constructs, can rescue both brain cell proliferation and attenuate microcephaly in *X. laevis* compared to drug treatment alone. This finding aligns with our in vitro work in cell culture, where forcing importin α to the cell cortex was able to rescue spindle misorientation (Figure 1I). These results demonstrate that the membrane localization of importin α is sufficient to rescue palmitoylation disruption-induced spindle misorientation in vitro and microcephaly in vivo.

Discussion

Importin α is primarily recognized as a nuclear transport protein during interphase and as a spindle assembly factor in mitosis by binding NLS sequence-containing proteins. In interphase, importin α binds to NLS sequence containing proteins and transports them into the nucleus, while in mitosis importin α binds to NLS sequence-containing proteins and transports them to the developing spindles at the midline of the cell (Takeda et al., 2011; Oka and Yoneda, 2018; Goldfarb et al., 2004). In the present study we have demonstrated a previously uncharacterized role for importin α at the PM. We have shown that importin α, when partitioned to the PM via

palmitoylation, plays a crucial role in mitotic spindle orientation. Disruption of importin α palmitoylation resulted in mitotic spindle misorientation and mislocalization of the aMT anchoring protein NuMA. While LGN and Gαi are necessary to ensure proper spindle orientation in metaphase (Bergstralh et al., 2017; Neville et al., 2022; Zhong et al., 2022), we have shown that importin α, while palmitoylated, is also required for proper NuMA localization and in turn proper spindle orientation, irrespective of LGN and Gαi. Our finding that importin α plays a role in spindle orientation through interaction with the aMT anchoring complex is especially noteworthy in that importin α's ability to bind cargo is sensitive to the RanGTP gradient which emanates from the chromatin. As NuMA is a known cargo of importin α and has been shown in this work to interact with palmitoylated importin α at the polar cortex, this provides a regulatory pathway by which the localization of the chromatin and the RanGTP gradient can determine where aMTs are anchored. This relationship is able to explain the well-defined spatial organization of the aMT anchoring complex exclusively to the polar cortex which has been shown to be essential for proper spindle orientation (Bergstralh et al., 2017)(Figure 6).

Our results demonstrated that disruption of importin α palmitoylation leads to developmental defects in *X. laevis* embryos, specifically microcephaly. Defects in neurogenesis, in particular microcephaly, have long been linked to spindle misorientation(Taverna et al., 2014). Neuroprogenitors rely on proper spindle orientation to correctly align polarity cues which regulate cell fate determination in the developing brain (Taverna et al., 2014). During early neurogenesis, neuroprogenitors rely on several symmetric divisions to generate a large enough population of cells to later divide asymmetrically and differentiate into neurons. Spindle misorientation can cause neuroprogenitors to prematurely differentiate, depleting the pool of neuroprogenitors, resulting in an overall decrease in neuronal tissue and microcephaly (Taverna

et al., 2014; Razuvaeva et al., 2023). Expression of importin α modified with a CaaX motif, which is forced to the PM by farnesylation, effectively rescued both the spindle misorientation observed in HCT116 cells and the developmental defects observed in *X. laevis* embryos. These findings further emphasize the role of palmitoylated importin α in spindle orientation and neurogenesis. The observed rescues not only demonstrate importin α's involvement in aMT anchoring, but also that the spindle misorientation and microcephaly observed when palmitoylation was disrupted by Wnt-C59 treatment are not due to off-target effects and can be attributed, in part, to mislocalization of importin α from the PM, as those phenotypes are reversed by forcing importin α to the PM.

We propose an updated model for mitotic spindle orientation in which aMT anchoring at the cell cortex is mediated by palmitoylated importin α through its interaction with NuMA (Figure 6). In this newly proposed model, the RanGTP gradient plays a significant role in limiting the binding of NuMA to palmitoylated importin α to the polar cortex exclusively. This provides a mechanism by which palmitoylated importin α can regulate spindle orientation by binding directly to NuMA with spatial binding cues provided by the RanGTP gradient emanating from the chromosomes at the metaphase plate (Figure 6). Notably, our newly proposed model provides a mechanistic link between factors known to affect spindle orientation, such as cell size, shape, and stretch, and the localization of aMT anchoring proteins. Given that palmitoylated importin α and its interaction with RanGTP is essential for proper localization of the aMT anchoring complex, these factors known to affect spindle orientation must exert their influence, at least in part, through palmitoylated importin α. Further studies to explore NuMA activation via phosphorylation, which has been previously linked with NuMA PM localization and association with the aMT anchoring complex of proteins (Gallini et al., 2016), and its impact on

539 binding to palmitoylated importin α would be beneficial to expand this model and provide a
540 robust view of NuMA localization in mitosis. It is reasonable to hypothesize that phosphorylated
541 NuMA could bind with differential preference to palmitoylated importin α similar to our
542 observation that hyper-palmitoylation of importin α increased NuMA/importin α interaction, but
543 this warrants further study and remains speculative.

544 The present work not only highlights the importance of importin α as a key upstream
545 regulator in mitotic spindle orientation, but also serves as the first evidence of a novel protein
546 transport pathway by which palmitoylated importin α can transport NLS containing proteins to
547 the PM. This new transport pathway could be involved in several cellular processes due to the
548 abundance of NLS containing proteins that enrich at the PM and provides a potential new level
549 of regulation of these processes through regulation of importin α palmitoylation. Overall, our
550 work challenges the long-standing dogma of importin α only facilitating transport into the
551 nucleus and suggests that there are a number of potential non-canonical roles for importin α at
552 the membrane.

553

554 **Acknowledgements**

555 We thank Natalie Mosqueda, Kathryn Malone, and Melanie Garcia for their constructive
556 feedback on this work, engaging discussions, and edits during the writing of this manuscript. We
557 thank Maurice Kernan, Holly Colognato, Gerald Thomsen, and Daniel Levy for their insights
558 and suggestions on experimental approach. We thank the Stony Brook University Central
559 Microscopy Imaging Center (CMIC) and Guowei Tian for assistance in imaging with Zeiss LSM
560 980 Airsycan 2 NLO Two-Photon Confocal Microscope. Work was supported by National
561 Institutes of Health grant 1R35GM147569-01 (C.W.B).

562

563 **Author Contributions**

564 C.W.B initially conceptualized the project. P.J.S and C.W.B designed the project. P.J.S performed
565 the majority of experiments and all analysis of data. N.M performed co-immunoprecipitation
566 experiments. P.J.S prepared the figures, and P.J.S and C.W.B wrote the manuscript. P.J.S, C.W.B
567 and N.M edited and revised the manuscript. C.W.B procured funding for this project.

568

569 **Declaration of Interests**

570 The authors declare no competing interests.

571

572 **Figures**

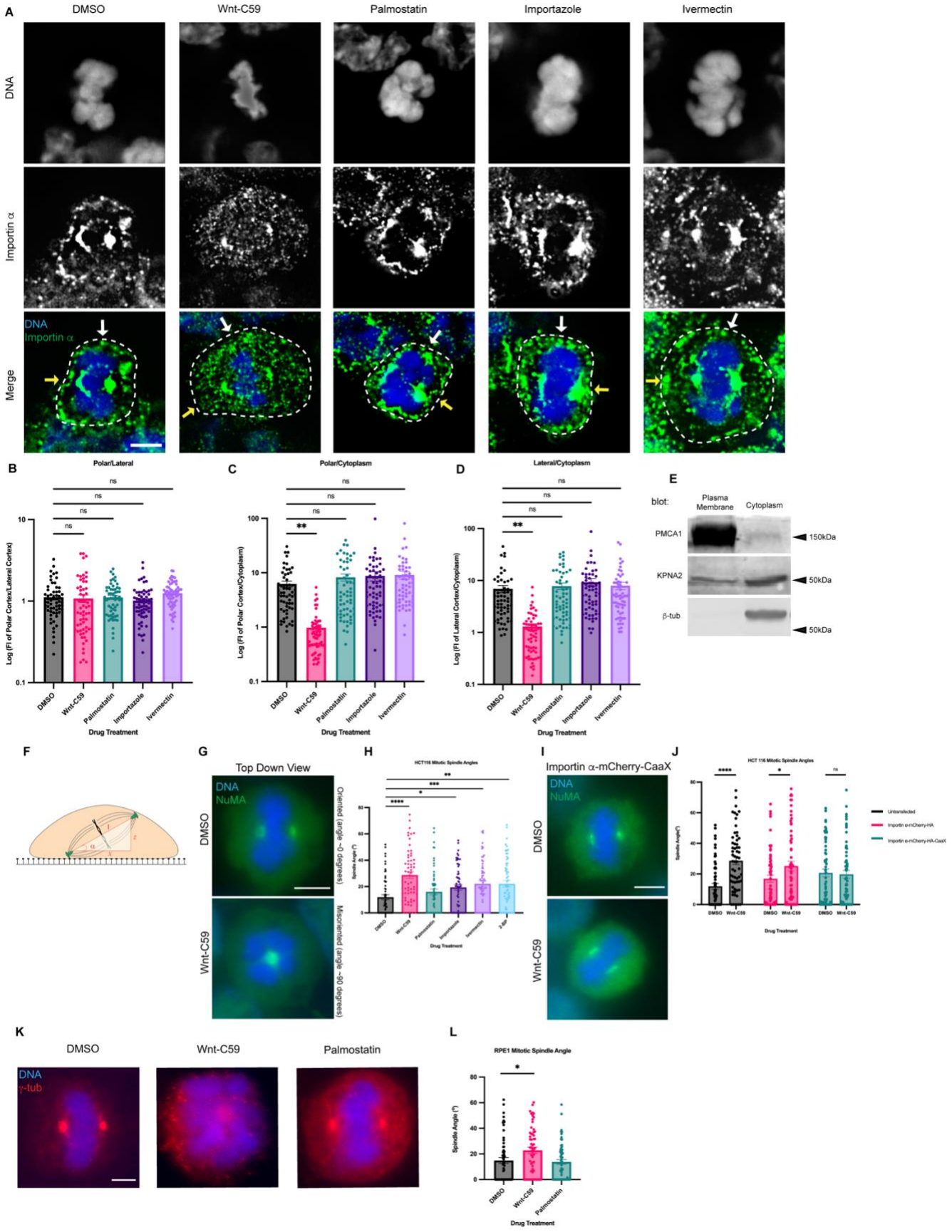

573

Figure 1. Palmitoylation Mediated Cortical Localization of Importin α and Importin α Cargo Binding are Required for Proper Mitotic Spindle Orientation.

A) Immunofluorescence images of importin α localization in metaphase-arrested (refer to Materials & Methods) HCT116 cells incubated for 1 hour with DMSO, drugs that inhibit importin palmitoylation (10μM Wnt-C59) drugs that enhance importin palmitoylation (50μM palmostatin), and drugs that inhibit importin cargo binding (25μM ivermectin) or cargo release (40μM importazole). Yellow arrows indicate cortical poles and white arrows indicate lateral cortex. Scale bar=5μm. Cell boundaries determined by brightfield.

B-D) Quantification of importin α localization in drug treated cells. Measurements of importin α signal intensity were made at three cellular locations: polar cortex, lateral cortex and cytoplasm. Polar cortex measurements were made for each cell at the pole with the higher measure of intensity, a similar method was used for lateral cortex measurements and cytoplasm measurements were made at the midline of the cell. These measurements were normalized to each other on a cell-by-cell basis by determining the ratio of cortical vs lateral importin α, cortical vs cytosolic importin α, and lateral vs cytosolic importin α. Mean +/- SEM n=60 from 2 replicates **=$p<0.01$ determined by Student's t-test.

E) Western blot of HCT116 cell fractions following subcellular fractionation to separate PM, cytoplasmic, organelle, and nuclear fractions. PM and cytoplasmic fractions shown. Western blots were immunostained for PMCA1 (PM marker), β-tubulin (cytoplasmic marker), and importin α (KPNA2).

F) Cartoon representation of a metaphase cell with misoriented spindles mounted on a coverslip indicating the angle, α, which was measured as the arctangent of the horizontal distance, z, over

the vertical distance, x, between the two centrosomes to determine the angle of spindle structures.

G) Immunofluorescence images of metaphase-arrested HCT116 cells in presence of DMSO or 10μM Wnt-C59 stained for NuMA. DMSO treated cell represents a properly oriented cell with a spindle angle of 0 degrees relative to the parallel of the coverslip the cells were mounted on. Wnt-C59 treated cell represents a severely misoriented cell with a spindle angle of 90 degrees relative to the parallel of the coverslip the cells were mounted on. Scale bar=5μm

H) Quantification of mitotic spindle angles for metaphase-arrested HCT116 cells incubated in DMSO, 10μM Wnt-C59, 50μM palmostatin, 40μM importazole, 25μM ivermectin, or 100μM 2-bromopalmitate for 1 hour prior to analysis. All drug treatments except palmostatin significantly increased the mean spindle angle of metaphase cells relative to a DMSO control. Mean +/- SEM, n=60 mitotic cells from 2 replicates *=$p<0.05$ **=$p<0.01$ ***=$p<0.001$ ****=$p<0.0001$ determined by Student's t-test. Refer to Materials & Methods for method of determining spindle angle.

I) Immunofluorescence images of metaphase-arrested HCT116 cells transfected via nucleofection with importin α-mCherry-HA-CaaX and incubated in either DMSO or 10μM Wnt-C59 for 1 hour prior to analysis stained for NuMA. Scale bar=5μm.

J) Quantification of mitotic spindle angles for metaphase-arrested HCT116 cells incubated with DMSO or 10μM Wnt-C59 expressing importin α-mCherry-HA or importin α-mCherry-HA-CaaX. Cells expressing importin α-mCherry-HA-CaaX showed no spindle misorientation when treated with Wnt-C59. Mean +/- SEM, n=60 mitotic cells from 2 replicates *=$p<0.05$ ****=$p<0.0001$ determined by Student's t-test.

618 K) Immunofluorescence images of metaphase-arrested RPE-1 cells incubated with DMSO,
619 10μM Wnt-C59, or 50μM palmostatin for 1 hour prior to analysis stained for γ-tubulin. DMSO
620 treated cells are representative of cells with properly oriented spindles. Wnt-C59 treated cells
621 were significantly misoriented and palmostatin treated cells were properly oriented when
622 compared to DMSO control. Scale bar=5μm
623 L) Quantification of mitotic spindle angles for metaphase-arrested RPE-1 cells incubated with
624 DMSO, 10μM Wnt-C59 or 50μM palmostatin for 1 hour prior to analysis. Wnt-C59 treatment
625 significantly increased the mean spindle angle of metaphase cells relative to a DMSO control
626 while palmostatin treatment did not significantly increase the mean spindle angle relative to a
627 DMSO control. Mean +/- SEM, n=60 mitotic cells from 2 replicates *=$p<0.05$ determined by
628 Student's t-test.
629

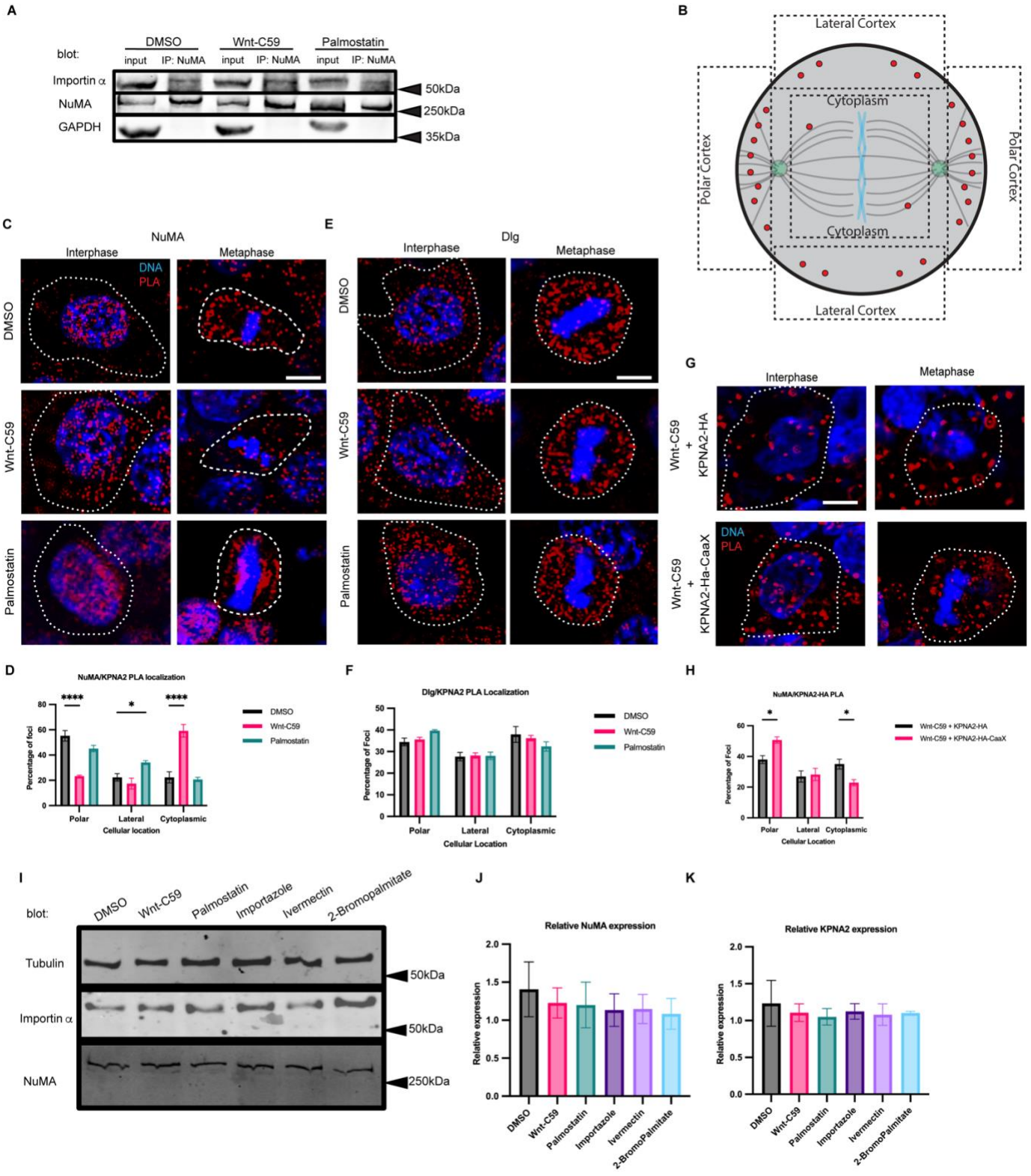

Figure 2. Importin α Interacts with NuMA, but not Dlg at the Metaphase Cell Cortex in a Palmitoylation Dependent Manner.

A) Western blot of NuMA immunoprecipitation from HCT116 cells treated with DMSO, 10μM Wnt-C59 or 50μM palmostatin for 1 hour prior to analysis. Immunoprecipitation of NuMA followed by importin α and NuMA western blot.

B) Schematic of PLA quantification. ROIs of quantification represented by dashed lines.

C) Immunofluorescence images of DuoLink proximity ligation assay (PLA) probing interaction of NuMA with importin α (KPNA2) in interphase and metaphase-arrested HCT116 cells in the presence of DMSO, 10μM Wnt-C59 or 50μM palmostatin for 1 hour prior to analysis. White dashed lines indicate cell borders as determined by brightfield images. Scale bar=5μm.

D) Quantification of the percentage of importin α (KPNA2)-NuMA PLA foci at the polar cortex, lateral cortex and cytoplasm in DMSO, Wnt-C59 and palmostatin-treated cells. Foci were enriched at the polar cortex in DMSO treated cells, the cytoplasm in Wnt-C59 treated cells, and the lateral cortex in palmostatin treated cells. Mean +/- SEM, n>136 foci *=$p<0.05$ ****=$p<0.0001$ determined by Student's t-test.

E) Immunofluorescence images of DuoLink PLA probing interaction of Dlg with importin α (KPNA2) in interphase and metaphase-arrested HCT116 cells in the presence of DMSO, 10μM Wnt-C59 or 50μM palmostatin. White dashed lines indicate cell borders. Scale bar=5μm.

F) Quantification of the percentage of importin α (KPNA2)-Dlg PLA foci at the polar cortex, lateral cortex and cytoplasm in DMSO, Wnt-C59 and palmostatin treated cells. Localization of PLA foci did not change across three drug treatments. Mean +/- SEM, n>297 foci, all data points are non-significant as determined by Student's t-test.

G) Immunofluorescence images of DuoLink proximity ligation assay probing interaction of NuMA with nucleofected importin α constructs (KPNA2-HA-mCherry and KPNA2-HA-mCherry-CaaX) in interphase and metaphase-arrested HCT116 cells in the presence of DMSO or

10μM Wnt-C59 for 1 hour prior to analysis. White dashed lines indicate cell borders as determined by brightfield images. Scale bar=5μm.

H) Quantification of the percentage of nucleofected importin α constructs(KPNA2)-NuMA PLA foci at the polar cortex, lateral cortex and cytoplasm in Wnt-C59 treated cells. Cells nucleofected with KPNA2-HA and treated with Wnt-C59 did not exhibit enrichment of foci at the PM and instead showed foci throughout the cell. Cells nucleofected with KPNA2-HA-CaaX and treated with Wnt-C59 exhibited foci enrichment at the PM indicating that expression of KPNA2-HA-CaaX rescued the effects of Wnt-C59 treatment. Mean +/- SEM, n>195 foci *=$p<0.05$ determined by Student's t-test.

I) Western blot of importin α, NuMA and β-tubulin in metaphase-arrested HCT116 cells in the presence of DMSO, 10μM Wnt-C59, 50μM Palmostatin, 40μM importazole, 25μM ivermectin, or 100μM 2-bromopalmitate.

J and K) Quantification of NuMA and importin α (KPNA2) expression levels respectively, relative to β-tubulin protein levels for each condition.

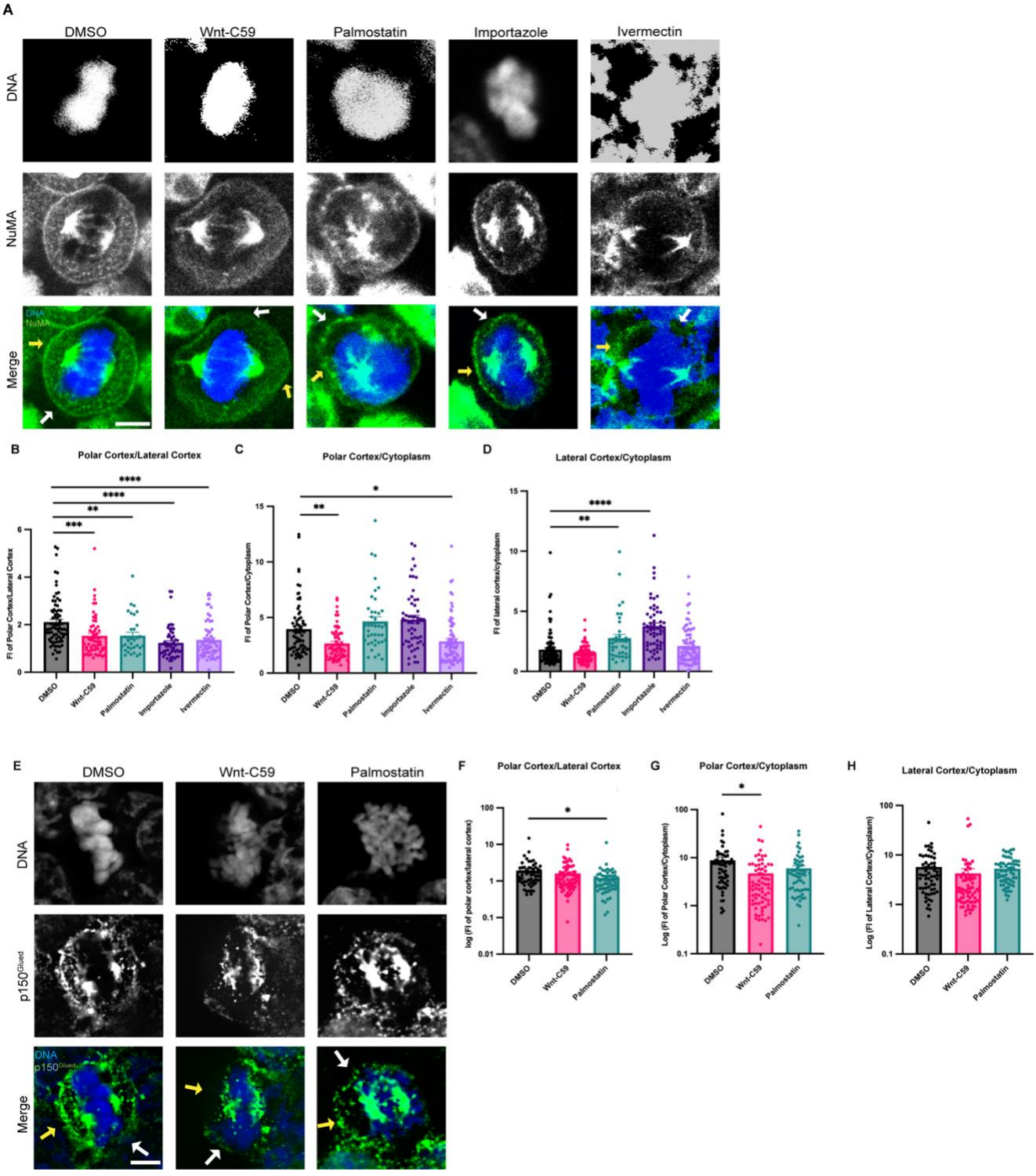

671

672 **Figure 3. Palmitoylated Importin α Regulates Cortical Localization of NuMA and**

673 **Dynein/Dynactin in Metaphase.**

A) Confocal images of NuMA localization in metaphase-arrested HCT116 cells in the presence of DMSO, 10μM Wnt-C59, 50μM palmostatin, 40μM importazole or 25μM ivermectin. Yellow arrows indicate cortical poles and white arrows indicate lateral cortex. Scale bar=5μm.

B-D) Quantification of NuMA localization in drug treated cells. Measurements of NuMA signal intensity were made at three cellular locations: polar cortex, lateral cortex and cytoplasm. Polar cortex measurements were made for each cell at the pole with the higher measure of intensity, a similar method was used for lateral cortex measurements and cytoplasm measurements were made at the midline of the cell. These measurements were normalized on a cell-by-cell basis by determining the ratio of polar vs lateral NuMA, polar vs cytosolic NuMA, and lateral vs cytosolic NuMA. Mean +/- SEM n>40 *=p<0.05 **=p<0.01 ***=p<0.001 ****=p<0.0001 determined by Student's t-test.

E) Immunofluorescence images of $p150^{Glued}$ localization in metaphase-arrested HCT116 cells treated with either DMSO, 10μM Wnt-C59, or 50μM palmostatin. Yellow arrows indicate cortical poles and white arrows indicate lateral cortex. Scale bar=5μm.

F-H) Quantification of $p150^{Glued}$ localization in drug-treated cells. Measurements of $p150^{Glued}$ signal intensity were made at three cellular locations: polar cortex, lateral cortex and cytoplasm. Polar cortex measurements were made for each cell at the pole with the higher measure of intensity, the same method being used for lateral cortex measurements and cytoplasm measurements at the midline of the cell. These measurements were normalized on a cell-by-cell basis by determining the ratio of polar vs lateral $p150^{Glued}$, polar vs cytosolic $p150^{Glued}$, and lateral vs cytosolic $p150^{Glued}$. Mean +/- SEM n=60 *=p<0.05 determined by Student's t-test.

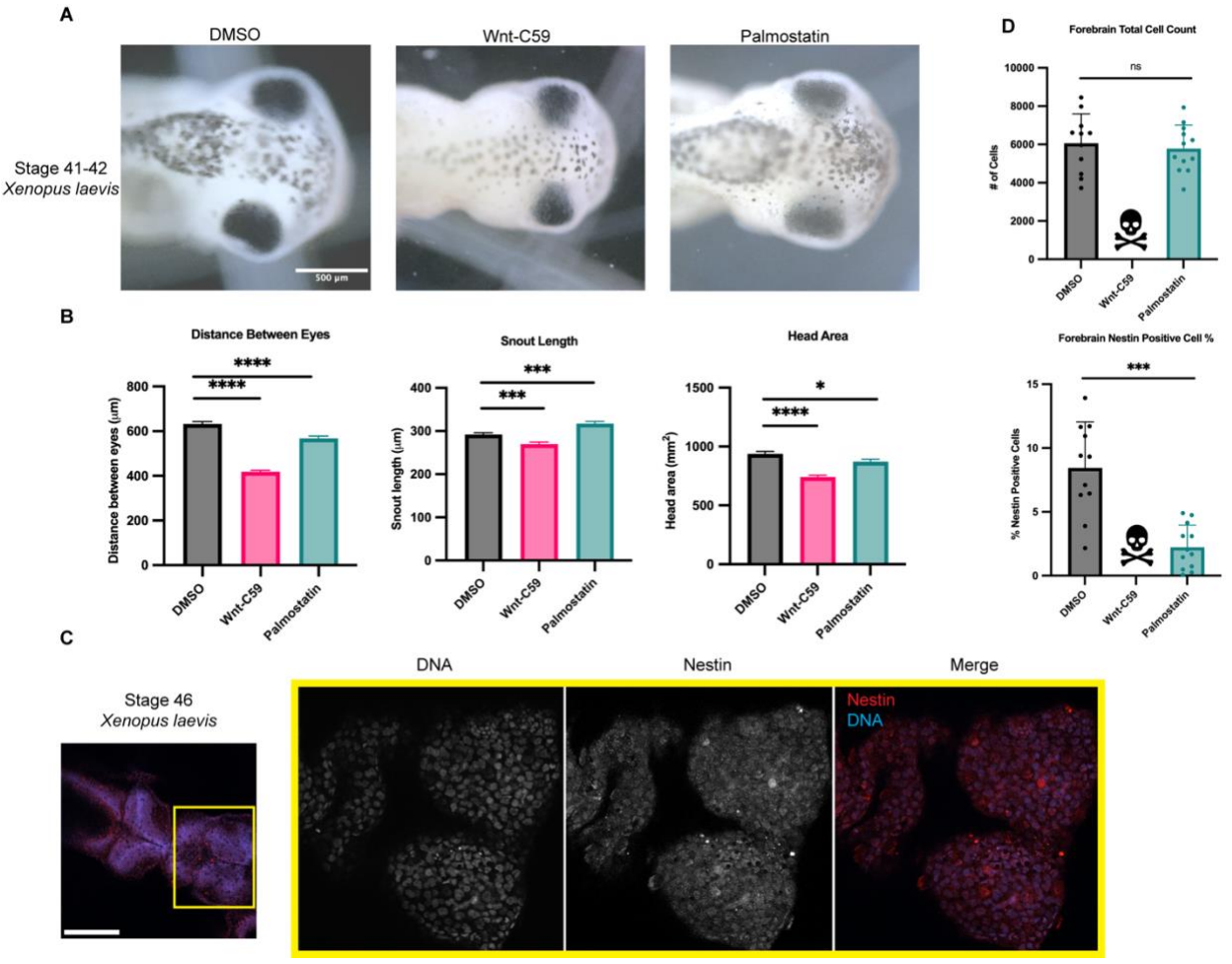

Figure 4. Regulation of Palmitoylation is Required for Proper Brain Development in *Xenopus laevis*.

A) Bright field images of NF stage 42 *X. laevis* grown in the presence of DMSO, 100µM Wnt-C59 or 1mM palmostatin. Scale bar=500µm

B) Measurements of drug treated stage 42 *X. laevis* head shape by 3 metrics: distance between eyes, snout length, and overall head area. All 3 metrics of head shape were significantly altered from DMSO control in both Wnt-C59 and palmostatin treatments. Mean +/- SEM n>55 *=p<0.05 ***=p<0.001 ****=p<0.0001 determined by Student's t-test.

C) Immunofluorescence images of DMSO treated NF stage 46 *X. laevis* immunostained for the neuroprogenitor marker nestin and stained with Hoechst to visualize DNA. Scale bar=250µm.

D) Quantification of total cell count in forebrains and percentage of forebrain cells positive for nestin signal in NF stage 46 *X. laevis* grown in the presence of DMSO, 100μM Wnt-C59 or 1mM palmostatin. Quantifications were performed on maximum projection images from z-stack images of *X. laevis* brains with a parent-child analysis to determine the number of total cells as determined by Hoechst signal that also were positive for nestin signal. All Wnt-C59 treated *X. laevis* embryos died before reaching NF stage 46 while all palmostatin treated *X. laevis* display a significantly reduced neuroprogenitor population by nestin positive cell count. Mean +/- SEM n=12 ***=$p<0.001$ determined by Student's t-test.

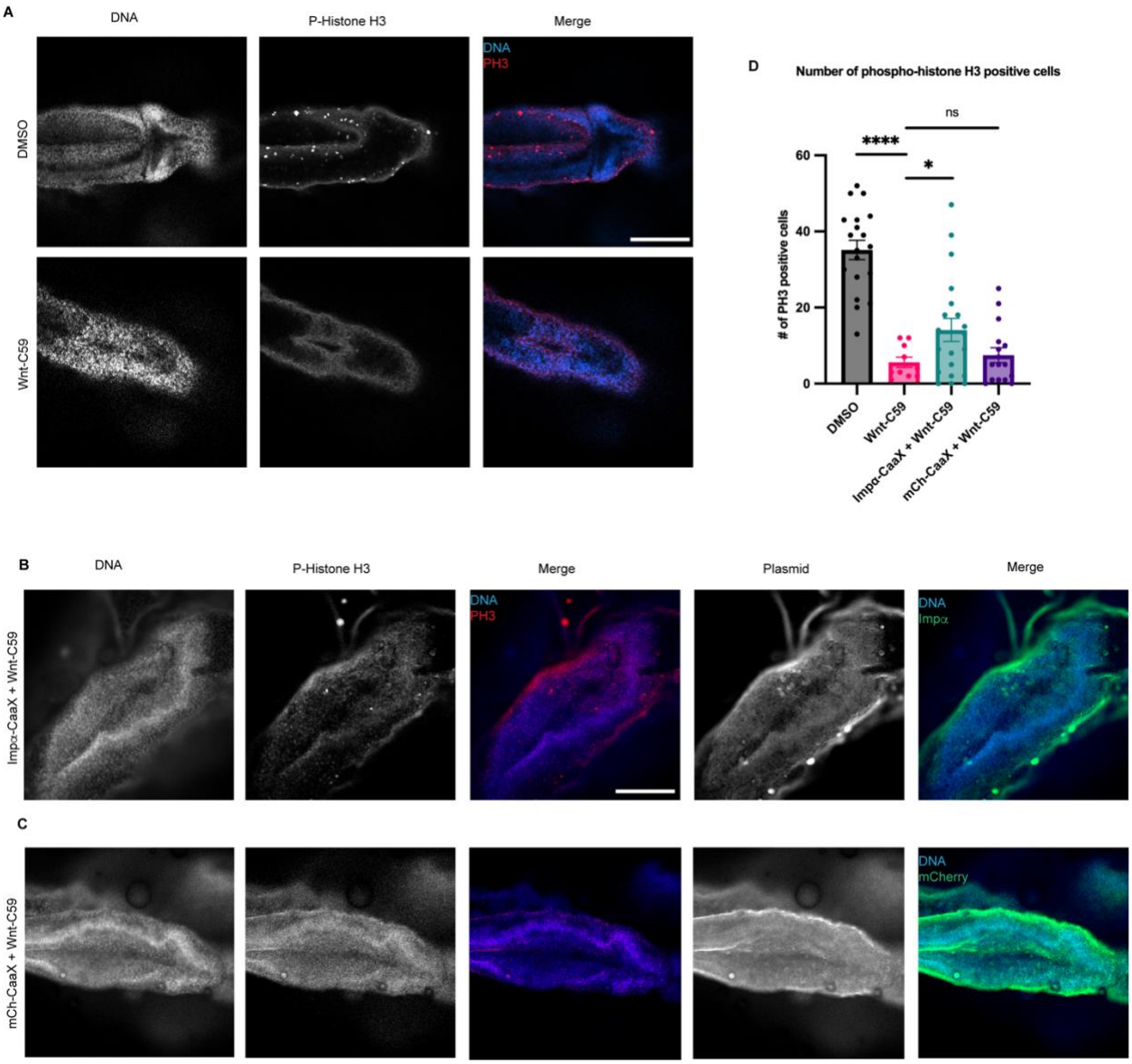

Figure 5. Overexpression of CaaX Modified Importin α in the Developing *X. laevis* Brain Partially Rescues Developmental Defects due to PORCN Inhibition.

A) Confocal images of NF stage 42 *X. laevis* brains from *X. laevis* grown in the presence of DMSO or 100μM Wnt-C59 immunostained for phospho-histone H3, a marker of actively dividing cells. Scale bar = 250μm.

B) Confocal images of NF stage 42 *X. laevis* brains from *X. laevis* expressing importin α modified with a c-terminal CaaX domain which forces cortical localization via farnesylation and

grown in the presence of 100μM Wnt-C59 immunostained for phospho-histone H3 and the modified importin α-CaaX construct.

C) Confocal images of NF stage 42 *X. laevis* brains from *X. laevis* expressing an mCherry construct modified with a c-terminal CaaX domain and grown in the presence of 100μM Wnt-C59 immunostained for phospho-histone H3 and the modified CaaX construct.

D) Quantification of the number of phospho-histone H3 positive cells in stage 42 *X. laevis* brains of *X. laevis* grown in the presence of DMSO or 100μM Wnt-C59 and expressing importin α-CaaX or mCherry-CaaX. Wnt-C59 treated *X. laevis* embryos showed a significantly reduced number of phospho-histone H3 positive cells in the brain compared to DMSO treated *X. laevis*. *X. laevis* embryos expressing importin α-CaaX in the brain display a partial rescue of the reduced phospho-histone H3 levels which was not recapitulated in *X. laevis* expressing mCherry-CaaX. Mean +/- SEM n>10 *=p<0.05 ****=p<0.0001 determined by Student's t-test.

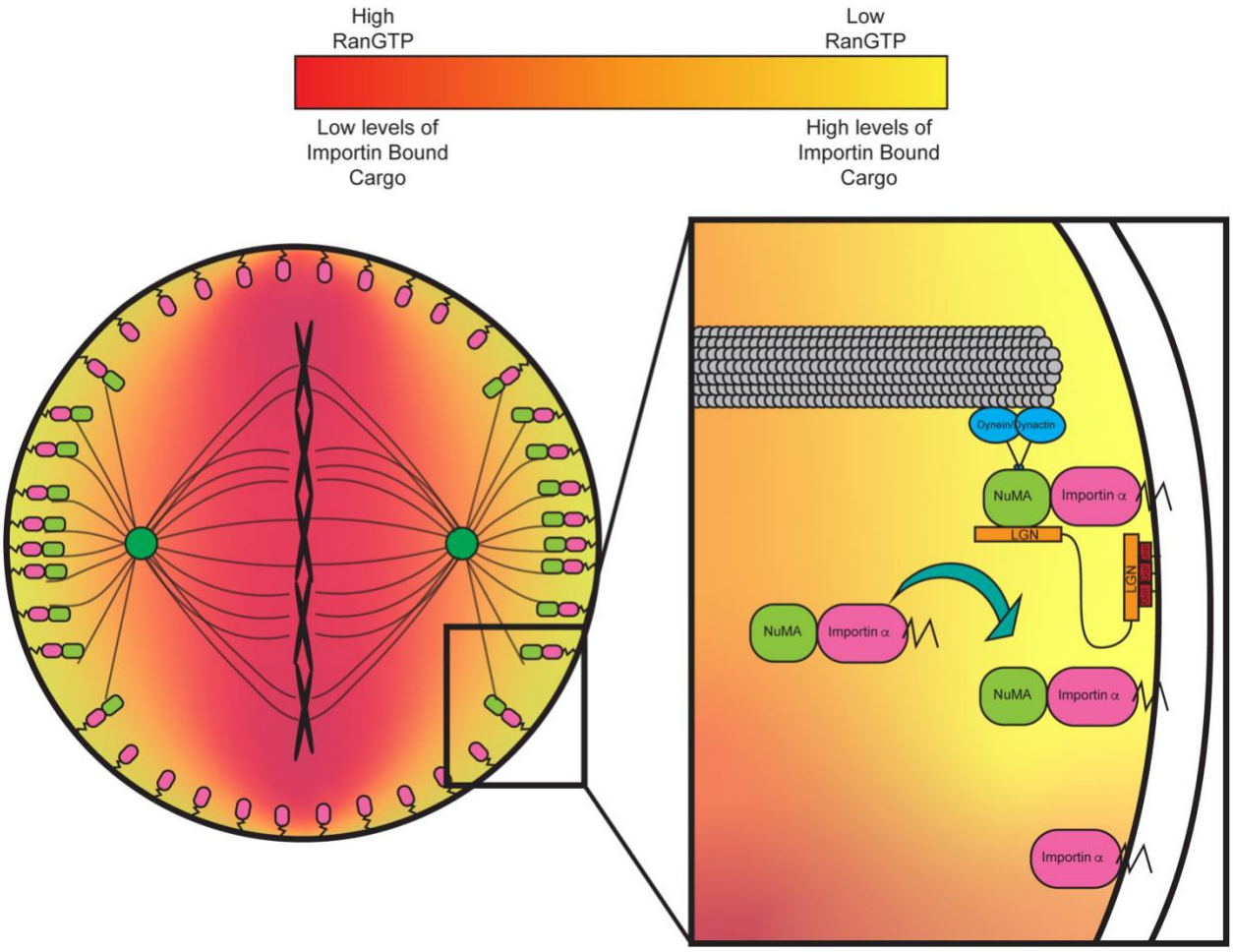

Figure 6. Importin α regulates mitotic spindle orientation through mediating NuMA localization to the metaphase cortex and maintenance at the cell cortex through anaphase in a palmitoylation dependent manner.

Proposed model of palmitoylated importin α's role in astral microtubule anchoring as a transporter of NuMA and a scaffold at the cell cortex for astral microtubule anchoring proteins to maintain cortical localization throughout metaphase and anaphase.

RESOURCE AVAILABILITY

Lead Contact for Reagent and Resource Sharing

Further information and requests for resources and reagents should be directed to and will be fulfilled by the Lead Contact, Christopher W. Brownlee (Christopher.Brownlee@stonybrook.edu).

Materials Availability

Plasmids generated in this study are being deposited to Addgene.

Data and Code Availability

- Microscopy data reported in this study will be shared by the lead contact upon request
- No original code was generated in this study
- Any additional information required to reanalyze the data reported in this paper is available from the lead contact upon request

MATERIALS AND METHODS

Reagents and Tools table

Reagent/Resource	Reference or Source	Identifier or Catalog Number
Experimental Models		
hTERT RPE-1 (human)	ATCC	CRL-4000
HCT 116 (human)	ATCC	CRL-4000
Xenopus laevis	NXR	N/A
Recombinant DNA		
Plasmid: Importin α-mCherry-CaaX	This study	N/A
Plasmid: Importin α-mCherry	This study	N/A
Plasmid: mCherry-CaaX	This study	N/A

Plasmid: Importin α-mCherry-CaaX (tet inducible)	This study	N/A
Plasmid: Importin α-mCherry (tet inducible)	This study	N/A
Plasmid: mCherry-CaaX (tet inducible)	This study	N/A
Plasmid: pcDNA6TR	Invitrogen T-Rex system from Thermofisher	Cat # V102520
Plasmid: pEGFP-C1-NuMA	Addgene	Cat # 81029
Plasmid: UBC::Importin α-mCherry-HA-CaaX	This study	N/A
Plasmid: UBC::Importin α-mCherry-HA-CaaX	This study	N/A
Antibodies		
Rabbit Polyclonal anti-NuMA	Novus Biologicals	Cat # NB100-74636
Rabbit Polyclonal anti-nestin	Sino Biological	Cat # 100244-T08
Monoclonal mouse living colors antibody	Takarabio	Cat # 632460
Rabbit polyclonal anti-mCherry	Proteintech	Cat # 26765-1-AP
Monoclonal mouse anti-importin α	Proteintech	Cat # 66870-1-Ig
Rabbit polyclonal anti-importin α	ABclonal	Cat # A1623
Monoclonal mouse anti-β tubulin	DSHB	Antibody E7
Monoclonal mouse anti-phospho histone H3	Proteintech	Cat # 66863-1-Ig
Monoclonal mouse anti-SAP97	Enzo Life Sciences	Cat # 06021547
Rabbit polyclonal anti-γ tubulin	Sigma-Aldrich	Cat # T5192
Monoclonal mouse anti-HA	Sigma-Aldrich	Cat # SAB2702196
Donkey anti-mouse IgG-AF488	Southern Biotech	Cat # 6411-30
Donkey anti-rabbit IgG-AF488	Southern Biotech	Cat # 6440-30

Donkey anti-mouse IgG-AF568	Invitrogen	Cat # A10037
Donkey anti-rabbit IgG-AF568	Invitrogen	Cat # A10042
Oligonucleotides and other sequence-based reagents		
Chemicals, Enzymes and other reagents		
Palmostatin-B	Sigma-Aldrich	Cat # 178501-5MG
Wnt-C59	Selleck Chem	Cat # S7037
Importazole	Selleck Chem	Cat # S8446
Ivermectin	ThermoFisher	Cat # J6277.03
2-BromoPalmitate	Sigma-Aldrich	Cat # 21604-1G
MG-132	Abcam	Cat # Ab141003
RO-3306	VWR International	Cat # 102516-266
McCoy's 5A Media	Avantor Scientific	Cat # 45000-374
Fetal bovine serum (FBS)	Avantor Scientific	Cat # 76327-086
PBS	Avantor Scientific	Cat # 45000-446
Gentamycin	Avantor Scientific	Cat # 102614-744
Duolink® *In Situ* Detection Reagents Red	Sigma-Aldrich	Cat # DUO92008
SE cell line 4D nucleofector X kit S	Lonza Bioscience	Cat # V4XC-1032
Software		
Celleste image analysis software version 6.0	Invitrogen	Cat # AMEP4942
Other		
Lonza 4D Nucleofector X-unit	Lonza Bioscience	Cat # AAF-1003X

Methods and Protocols

Cell culture

RPE-1 and HCT116 cells were cultured as previously described (Kiyomitsu and Cheeseman, 2012).

Animal models

Adult Female XLA.NXR-WTNXR (NXR_0031) frogs were purchased from the National Xenopus Resource and maintained at the Stony Brook University animal facility. Frogs were maintained in a pathogen-free facility held at 18°C, housed socially in aquatic tanks under 12:12h light:dark cycles and fed three times weekly with a pelleted Xenopus diet. All experimental procedures were approved by the Institutional Animal Care and Use Committee. All animals were maintained in accordance with standards established by the Division of Laboratory Animal Resources at Stony Brook University

Cell culture and immunostaining

RPE-1 and HCT116 cells were cultured as previously described (Kiyomitsu and Cheeseman, 2012) in DMEM F-12 and McCoy's 5A media, respectively, supplemented with 5% FBS and grown at 5% CO_2. Immunostaining was carried out on cells cultured onto fibronectin coated coverslips, fixed with 4% PFA, permeabilized with PBS+0.2% Triton X-100 (Sigma-Aldrich 9036-19-5), and blocked with Bovine Serum Albumin (BSA) in PBS+0.2% Triton X-100. The coverslips were than incubated with antibodies diluted in PBS+0.2% Triton X-100 as follows: Rabbit polyclonal anti-NuMA 1:1000 (Novus Biologicals), monoclonal living colors antibody 1:1000 (Takarabio), rabbit polyclonal anti-mcherry 1:1000 (Proteintech), monoclonal anti-importin α 1:1000 (Proteintech), rabbit polyclonal anti-importin α 1:1000 (ABclonal), monoclonal anti-β tubulin E7 1:1000 (DSHB), monoclonal anti-SAP97 1:1000 (Enzo Life Sciences), rabbit polyclonal anti-γ tubulin 1:1000 (Sigma-Aldrich), donkey anti-mouse IgG AF-

488 1:1000 (Southern Biotech), donkey anti-rabbit IgG AF-488 1:1000 (Southern Biotech), donkey anti-mouse IgG AF-568 1:1000 (Invitrogen) and donkey anti-rabbit IgG AF-488 1:1000 (Invitrogen). The coverslips were then mounted onto slides with ProLong Diamond Antifade Mountant (ThermoFisher P36961).

Mitotic arrest and drug treatment

RPE-1 and HCT116 cells were arrested in metaphase through a sequential drug treatment of RO-3306 and MG-132. Cells were treated with 9μM RO-3306 to arrest at the G2/M transition for 20 hours at 37°C. Cells were then washed with fresh media three times to remove RO-3306 and treated with 20μM MG-132 within 15 minutes of RO-3306 washout to arrest cells at metaphase. Cells were incubated in MG-132 for 1 hour at 37°C. In experiments with palmitoylation and importin function disrupting drug treatments cells were treated with DMSO, 10μM Wnt-C59, 50μM palmostatin, 40μM importazole, 25μM ivermectin, or 100μM 2-bromopalmitate with the MG-132 treatment and incubated for 1 hour at 37°C.

Spindle angle measurement

Mitotic spindle angles of metaphase-arrested cells were determined by measuring the vertical and horizontal distances between the centrosomes at each pole of the mitotic cell and calculating the arctangent of the vertical distance divided by the horizontal distance as follows:

$$\alpha = \arctan\left(\frac{z}{x}\right)$$

The vertical distance was determined through imaging the cell and measuring the length of a line drawn between each centrosome. The horizontal distance was determined through using a z-stack of the mitotic cell, determining at which z-slice each centrosome was in optimal focus, and calculating the z distance between each slice of optimal focus. Z-stacks were taken at a step distance of 0.1μm with varying numbers of steps depending on individual cell size.

X. laevis fertilization

Xenopus laevis adult females were induced to lay eggs by a priming injection of 100 U of pregnant mare serum gonadotropin (PMSG) at least 48 hours before use and a boosting injection of 500 U of human chorionic gonadotropin (hCG) 16 hours before use. Following the hCG injection, adult female *X. laevis* were placed in a 2L water bath of 1X MMR (100 mM NaCl, 2 mM KCl, 1 mM $MgCl_2$, 2 mM $CaCl_2$, 0.1 mM EDTA, 5 mM HEPES pH 7.8) overnight at 17°C. approximately 16 hours following hCG injection, fresh eggs were collected by squeezing eggs from ovulating frogs into a 10cm plastic petri dish. To fertilize eggs, a sperm solution made from ¼ of a male frog testis was placed in 1mL 1X MR (100 mM NaCl, 1.8 mM KCl, 2.0 mM $CaCl_2$, 1.0 $MgCl_2$, 5.0 mM HEPES-NaOH, pH 7.6) and homogenized using scissors and a pestle. 1mL of sperm solution was added dropwise to the freshly squeezed eggs and the dish was swirled to form a monolayer of eggs and incubated for 3 mins. Dishes were flooded with milli-Q water and incubated for an additional 10 mins. Eggs were dejellied with a 2% cysteine solution for 6 minutes with occasional swirling and washed 5 times with 1/3 MR. Fertilized eggs were incubated at 23°C until the appropriate developmental stage. In experiments where *X. laevis* embryos were drug treated, the embryos were placed into a bath of 1/3 MR containing either DMSO, 100µM Wnt-C59, or 1mM palmostatin 24 hours post fertilization and kept in drug bath until the appropriate developmental stage for each experiment. In drug treatment conditions, morphometric defects made it often difficult to determine the exact stage of Wnt-C59 and palmostatin treated embryos between NF stages 40 to 43, so analysis was conducted when the DMSO treated embryos were at the appropriate stage.

X. laevis morphometric measurements

X. laevis embryos were analyzed for morphometric defects at stage 42 by immobilizing embryos in a bath of 140μg/mL MS-222 and imaging at 4X mounted upright. All measurements were made in ImageJ. Distance between eyes was determined by measuring the straight line distance from the right most portion of the left eye to the left most portion of the right eye, snout length was determined by drawing a line from the front of the left eye to the right eye and then measuring the straight line distance from the center of this line to the mouth, and overall head area was determined by measuring the area of a circle drawn around the head such that each eye is completely within the circle and the circle does not extend beyond the snout.

X. laevis whole mount immunostaining

X. laevis embryos were fixed in 4% PFA for 24 hours at 4ºC. Following fixation, embryos were immunostained by washing in PBS 3x20 min, photobleaching in a solution of 5% formamide and 1.2% hydrogen peroxide for 2 hours, washing in PBS + 0.1% Triton X-100 (PBST) overnight at 4ºC, blocking with 2% BSA in PBST for 3 hours at RT, incubating with 1º antibodies diluted in PBST overnight at 4ºC as follows: rabbit polyclonal anti-nestin 1:1000 (Sino Biological), rabbit polyclonal anti-mCherry 1:1000 (Proteintech), and monoclonal anti-phospho Histone H3 1:1000 (Proteintech), washing 3x1 hour in PBST, incubating with 2º antibodies diluted in PBST overnight at 4ºC as follows: , washing 3x1 hour in PBST and mounting onto a coverslip in fluoromount G. In cases where embryos were cleared before mounting, embryos were chilled in 1-propanol and incubated 2x5 minutes, cleared with 5mL Murray's (2 parts Benzyl Benzoate and 1 part Benzyl Alcohol) and then mounted onto a coverslip with fluoromount G.

Plasmid construct development

Plasmid constructs were cloned into pCS2+ and pcDNA4TO vectors from existing plasmid constructs of importin α, GFP, mCherry-CaaX, and NuMA-GFP.

857 **Embryo microinjection**

858 Plasmid was loaded into a needle pulled from a 1mm glass capillary tube (TW100F-3, World
859 Percision Instruments) using a L/M-3P-A electrode/needle puller. Embryos were placed in a
860 mesh-bottomed plastic dish with 2.5% Ficoll in 1/3 MR and microinjected with a 2nL droplet of
861 the appropriate plasmid using a Narishige IM-400 microinjector system equipped with a MM-3
862 micromanipulator (Narishige). For stage 1 injections embryos were injected directly at the
863 animal pole, for stage 2 injections 1 blastomere was injected at the animal pole, and for stage 5
864 injections the D11 blastomere was injected at roughly the middle of the blastomere (as per
865 Moody, 1987). pCS2+ plasmids were injected at a concentration of 10ng/µL such that the final
866 concentration of plasmid delivered was 20pg. pcDNA4TO plasmids were co-injected with
867 pcDNA6TR at concentrations of 5ng/µL and 25ng/µL respectively such that the final
868 concentration of total plasmid delivered was 60pg. Following injection, embryos were placed
869 into a new dish containing 2.5% Ficoll in 1/3 MR and incubated at 23°C for 4 hours after which
870 embryos were moved to a dish containing 1/3 MR and incubated at 23°C until appropriate
871 developmental stage. Embryos injected with pcDNA4TO + pcDNA6TR were placed in 1/3 MR
872 containing 12.5µg/mL doxycycline to induce gene expression 4 hours post injection and
873 transferred to fresh 1/3 MR with 12.5µg/mL doxycycline 24 hours post injection.

874 ***X. laevis* nestin positive cell count**

875 Stage 46 *X. laevis* embryos were whole mount fixed and stained for DNA (Hoechst) and nestin
876 (Rb α-nestin Sino Biological 100244-T08). Embryos were imaged at 20X magnification on an
877 EVOS M7000 epifluorescent microscope to generate a z-stack image of the brain of each
878 embryo. Z-stack images were processed in Celeste Image Analysis software for 3D-
879 deconvolution to remove background signal and using a parent child analysis measured the

880 number of DNA containing cells in the brain with overlapping nestin signal in the maximum
881 projection of the processed z-stack.

882 ***X. laevis* phospho-histone H3 positive cell count**

883 Stage 42 *X. laevis* embryos were whole mount fixed and stained for DNA (Hoechst), Phospho-
884 histone H3, and mCherry to visualize mCherry tagged proteins from microinjected constructs.
885 Whole embryos were imaged at 10X on a Zeiss LSM 980 confocal microscope by imaging a Z-
886 stack of the brain. A maximum projection image from this z-stack was then processed in Celeste
887 Image Analysis Software and a 3D count was measured in an ROI around the brain to determine
888 the number of cells positive for Phospho-histone H3 signal. Phospho-histone H3 positive cell
889 counts were determined by thresholding the minimal signal such that individual positive cells
890 could be resolved from background fluorescence.

891 **Proximity ligation assay**

892 Proximity ligation assay (PLA) was performed using DuoLink PLA (Millipore Sigma) following
893 the recommended protocol. PLA analysis of importin α and NuMA interaction was performed in
894 mitotically arrested HCT 116 cells using mouse anti-importin α (Proteintech) and rabbit anti-
895 NuMA (Novus Biologicals). PLA analysis of importin α and Dlg interaction was performed in
896 mitotically arrested HCT 116 cells using rabbit anti-importin α (ABclonal) and mouse anti-
897 SAP97 (Enzo Life Sciences). Cells were imaged with an EVOS M7000 epifluorescent
898 microscope at 60X magnification. Localization of PLA fluorescent signal was quantified by
899 counting the number of foci within three separate ROIs of each cell. Polar cortex ROI was
900 defined as the region from the plasma membrane at each pole to the centrosomes. Lateral cortex
901 ROI was defined as the region from the plasma membrane to the chromatin between the
902 centrosomes. Cytosol ROI was defined as the region between the centrosomes excluding the

plasma membrane. The number of foci in each region was calculated as a percentage of the total number of foci for that cell. Cell border was determined by a brightfield image of each mitotic cell quantified.

Cell lysis and western blot analysis

Lysates of RPE-1 and HCT 116 cells were generated from 10cm dishes seeded with $1x10^6$ cells 2 days prior to lysis. Cells were collected by washing with ice cold PBS and scraping off the plate into solution. Cells were spun at 100xg for 5 minutes, supernatant was aspirated and cells were resuspended in 150µL RIPA buffer (150 mM sodium chloride, 1.0% Triton X-100, 0.5% sodium deoxycholate, 0.1% SDS, 50 mM Tris, pH 8.0) supplemented with 10µg/mL each of leupeptin, pepstatin and chymostatin (LPC) protease inhibitors. Resuspended cells were rocked at 4°C for 1 hour and spun at 12,000 rpm for 20 minutes at 4°C in an Eppendorf FA-45-24-11 rotor. Supernatant containing cell lysate proteins was then mixed 1:1 with 2X laemlli buffer, boiled at 100°C for 5 minutes and stored at -20°C until use. Western blot analysis was performed on cell lysates by running lysates through SDS-PAGE in a 7.5% or 5.0% Tris-glycine gel (dependent on size of proteins being analyzed), transferring to a nitrocellulose membrane, and blotting for target proteins. Western blot analysis for NuMA was performed with overnight transfer of SDS-PAGE gel at 20V at 4°C while all other proteins were performed with a transfer at 150V for 90 minutes at room temperature.

Co-Immuno precipitation

Co-immunoprecipitation was performed with Thermo Fisher IgG conjugated magnetic Dynabeads following recommended protocol. Cell lysates were generated for immunoprecipitation experiments with previously stated cell lysis protocol using a non-

925 denaturing lysis buffer (20 mMTris HCl pH 8, 137 mM NaCl, 1% Triton X-100, 2 mM EDTA) in
926 place of RIPA buffer.

927 **Mitotic protein localization measurement**

928 To determine changes to KPNA2 and NuMA localization in cultured cells upon drug treatment,
929 cells were mounted onto fibronectin coated coverslips, arrested in metaphase, drug treated,
930 washed with cytoskeletal buffer (100mM NaCl, 300mM Sucrose, 3mM MgCl2, 10mM PIPES,
931 pH 6.9, supplemented with 250µL 1M EGTA and 250µL Triton X-100 per 50 mL immediately
932 before use), fixed with 4% PFA, and immunostained for DNA and KPNA2/NuMA. For KPNA2
933 localization cells were imaged using an EVOS M7000 at 100X with cell boundaries determined
934 using bright-field images. For NuMA localization cells were imaged using a Leica SP5 confocal
935 at 40X. To determine the cellular localization of target protein in each drug condition, 60 mitotic
936 cells were imaged per drug treatment and the fluorescent intensity of KPNA2 or NuMA signal
937 was measured in ImageJ at three cellular locations. A 10 pixel wide and 50 pixel long line was
938 drawn at one cortical pole, one lateral membrane, and along the midline of the cell and
939 measured. In order to normalize variations in intensity from inconsistent immunostaining, these
940 measurements were normalized to each other on a cell-by-cell basis by determining the ratio of
941 polar vs lateral signal, polar vs cytosolic signal, and lateral vs cytosolic signal. In the cases where
942 one cortical pole differed in intensity from the opposite cortical pole, the pole with the higher
943 measure of intensity was used for data analysis (the same method was used when measuring the
944 lateral poles).

945 **DNA transfection**

946 HCT116 cells were seeded onto fibronectin coated coverslips. The following day media was
947 replaced with serum free media and a mixture of 1µg plasmid in 12µL polyethylenimine (PEI)

was added dropwise to cells. Cells were incubated in PEI mixture for 4 hours then media was washed out and replaced with complete media and incubated overnight before fixation and imaging.

Subcellular fractionation

HCT116 cells were seeded in a 10cm dish and incubated at 37°C. Following 2 days of incubation Cells were incubated with DMSO for 1 hour at 37°C then lifted from dish with ice cold PBS and a cell scraper. Collected cells were then fractionated using the Minute Plasma Membrane/Protein Isolation and Cell Fractionation kit from Invent Biotechnologies following the recommended protocol.

DNA nucleofection

HCT116 cells were transfected via nucleofection using LONZA SE cell line 4D-Nucleofector kit (Catalog #V4XC-1032) following recommended protocol. Following nucleofection cells were incubated for 24 hours before fixation and immunostaining for mitotic spindle angle analysis.

Palmitoylation prediction

GPS-Palm (Ning et al., 2021) was employed for detection of potential palmitoylated cysteines within human KPNA2. Cysteines above a threshold score of >0.6 (specificity > 85% and accuracy > 82%) were considered to be likely palmitoylated.

Nuclear localization signal, cellular localization, and protein function prediction

NucPred (Brameier et al., 2007) was used to determine which proteins in the human genome contain potential NLS sequences. Any proteins above a threshold score of >0.63 (specificity > 71% and accuracy >53%) were considered potential NLS-sequence containing candidate proteins. Proteins were then filtered to discard transmembrane proteins while retaining only plasma membrane proteins, as identified by UniProt GO identifiers (Ashburner et al., 2000;

Aleksander et al., 2023). Proteins were then sorted by cellular localization and function using GO enrichment analysis (Thomas et al., 2022).

QUANTIFICATION AND STATISTICAL ANALYSIS

All statistical analysis was performed in GraphPad Prism 10.0. Comparisons between datasets was determined by a student's t-test unless otherwise stated. Graphs represent the mean value +/- the SEM unless otherwise stated. *p<0.05 **p<0.01 ***p<0.001 ****p<0.0001 unless otherwise stated.

References

Alam, S.M. 2018. Proximity Ligation Assay (PLA). *Curr Protoc Immunol*. 123. doi:10.1002/cpim.58.Proximity.

Aleksander, S.A., J. Balhoff, S. Carbon, J.M. Cherry, H.J. Drabkin, D. Ebert, M. Feuermann, P. Gaudet, N.L. Harris, D.P. Hill, R. Lee, H. Mi, S. Moxon, C.J. Mungall, A. Muruganugan, T. Mushayahama, P.W. Sternberg, P.D. Thomas, K. Van Auken, J. Ramsey, D.A. Siegele, R.L. Chisholm, P. Fey, M.C. Aspromonte, M.V. Nugnes, F. Quaglia, S. Tosatto, M. Giglio, S. Nadendla, G. Antonazzo, H. Attrill, G. Dos Santos, S. Marygold, V. Strelets, C.J. Tabone, J. Thurmond, P. Zhou, S.H. Ahmed, P. Asanitthong, D. Luna Buitrago, M.N. Erdol, M.C. Gage, M. Ali Kadhum, K.Y.C. Li, M. Long, A. Michalak, A. Pesala, A. Pritazahra, S.C.C. Saverimuttu, R. Su, K.E. Thurlow, R.C. Lovering, C. Logie, S. Oliferenko, J. Blake, K. Christie, L. Corbani, M.E. Dolan, L. Ni, D. Sitnikov, C. Smith, A. Cuzick, J. Seager, L. Cooper, J. Elser, P. Jaiswal, P. Gupta, S. Naithani, M. Lera-Ramirez,

995 K. Rutherford, V. Wood, J.L. De Pons, M.R. Dwinell, G.T. Hayman, M.L. Kaldunski, A.E.
996 Kwitek, S.J.F. Laulederkind, M.A. Tutaj, M. Vedi, S.J. Wang, P. D'Eustachio, L. Aimo, K.
997 Axelsen, A. Bridge, N. Hyka-Nouspikel, A. Morgat, S.R. Engel, K. Karra, S.R. Miyasato,
998 R.S. Nash, M.S. Skrzypek, S. Weng, E.D. Wong, E. Bakker, T.Z. Berardini, L. Reiser, A.
999 Auchincloss, G. Argoud-Puy, et al. 2023. The Gene Ontology knowledgebase in 2023.
1000 *Genetics*. 224:1–14. doi:10.1093/genetics/iyad031.
1001 Anjur-Dietrich, M.I., V. Gomez Hererra, R. Farhadifar, H. Wu, H. Merta, S. Bahmanyar, M.J.
1002 Shelley, and D.J. Needleman. 2024. Mechanics of spindle orientation in human mitotic cells
1003 is determined by pulling forces on astral microtubules and clustering of cortical dynein.
1004 *Dev. Cell*. doi:10.1016/j.devcel.2024.05.022.
1005 Ashburner, M., C.A. Ball, J.A. Blake, D. Botstein, H. Butler, J.M. Cherry, A.P. Davis, K.
1006 Dolinski, S.S. Dwight, J.T. Eppig, M.A. Harris, D.P. Hill, L.I.-T.A. Kasarskis, S. Lewis,
1007 J.C. Matese, J.E. Richardson, M. Ringwald, G.M. Rubin, and G. Sherlock. 2000. Gene
1008 Ontology: tool for the unification of biology. *Nat. Genet.* 25:25–29.
1009 doi:10.2174/138161282466618052210520 2.
1010 Bergstralh, D.T., N.S. Dawney, and D. St Johnston. 2017. Spindle orientation: A question of
1011 complex positioning. *Dev.* 144:1137–1145. doi:10.1242/dev.140764.
1012 Bergstralh, D.T., H.E. Lovegrove, I. Kujawiak, N.S. Dawney, J. Zhu, S. Cooper, R. Zhang, and
1013 D.S. Johnston. 2016. Pins is not required for spindle orientation in the drosophila wing disc.
1014 *Dev.* 143:2573–2581. doi:10.1242/dev.135475.
1015 Bergstralh, D.T., and D. St Johnston. 2014. Spindle orientation: What if it goes wrong? *Semin.*
1016 *Cell Dev. Biol.* 34:140–145. doi:10.1016/j.semcdb.2014.06.014.
1017 Bowman, S.K., R.A. Neumüller, M. Novatchkova, Q. Du, and J.A. Knoblich. 2006. The

Drosophila NuMA Homolog Mud Regulates Spindle Orientation in Asymmetric Cell Division. *Dev. Cell*. 10:731–742. doi:10.1016/j.devcel.2006.05.005.

Brameier, M., A. Krings, and R.M. MacCallum. 2007. NucPred - Predicting nuclear localization of proteins. *Bioinformatics*. 23:1159–1160. doi:10.1093/bioinformatics/btm066.

Brownlee, C., and R. Heald. 2019. Importin α Partitioning to the Plasma Membrane Regulates Intracellular Scaling. *Cell*. 176:805-815.e8. doi:10.1016/j.cell.2018.12.001.

Camuglia, J., S. Chanet, and A.C. Martin. 2022. Morphogenetic forces planar polarize LGN/Pins in the embryonic head during Drosophila gastrulation. *bioRxiv*. 2022.01.07.475359.

Carvalho, C.A., S. Moreira, G. Ventura, C.E. Sunkel, and E. Morais-De-Sá. 2015. Aurora a triggers Lgl cortical release during symmetric division to control planar spindle orientation. *Curr. Biol.* 25:53–60. doi:10.1016/j.cub.2014.10.053.

Chang, C.C., T.L. Huang, Y. Shimamoto, S.Y. Tsai, and K.C. Hsia. 2017. Regulation of mitotic spindle assembly factor NuMA by Importin-β. *J. Cell Biol.* 216:3453–3462. doi:10.1083/jcb.201705168.

Charnley, M., F. Anderegg, R. Holtackers, M. Textor, and P. Meraldi. 2013. Effect of Cell Shape and Dimensionality on Spindle Orientation and Mitotic Timing. *PLoS One*. 8. doi:10.1371/journal.pone.0066918.

Chhabra, S.N., and B.W. Booth. 2021. Asymmetric cell division of mammary stem cells. *Cell Div.* 16:1–15. doi:10.1186/s13008-021-00073-w.

Dekker, F.J., O. Rocks, N. Vartak, S. Menninger, C. Hedberg, R. Balamurugan, S. Wetzel, S. Renner, M. Gerauer, B. Schölermann, M. Rusch, J.W. Kramer, D. Rauh, G.W. Coates, L. Brunsveld, P.I.H. Bastiaens, and H. Waldmann. 2010. Small-molecule inhibition of APT1 affects Ras localization and signaling. *Nat. Chem. Biol.* 6:449–456.

doi:10.1038/nchembio.362.

Du, Q., and I.G. Macara. 2004. Mammalian Pins is a conformational switch that links NuMA to heterotrimeric G proteins. *Cell*. 119:503–516. doi:10.1016/j.cell.2004.10.028.

Elmaci, I., M.A. Altinoz, R. Sari, and F.H. Bolukbasi. 2018. Phosphorylated Histone H3 (PHH3) as a Novel Cell Proliferation Marker and Prognosticator for Meningeal Tumors: A Short Review. *Appl. Immunohistochem. Mol. Morphol.* 26:627–631. doi:10.1097/PAI.0000000000000499.

Ems-McClung, S.C., M. Emch, S. Zhang, S. Mahnoor, L.N. Weaver, and C.E. Walczak. 2020. RanGTP induces an effector gradient of XCTK2 and importin α/β for spindle microtubule cross-linking. *J. Cell Biol.* 219:1–15. doi:10.1083/jcb.201906045.

Exner, C.R.T., and H.R. Willsey. 2021. Xenopus leads the way: Frogs as a pioneering model to understand the human brain. *Genesis*. 59. doi:10.1002/dvg.23405.

Fankhaenel, M., F. Sadat Golestan Hashemi, M. Mosa Hosawi, L. Mourao, P. Skipp, X. Morin, C. LGJ Scheele, and S. Elias. 2023. Annexin A1 is a polarity cue that directs planar mitotic spindle orientation during mammalian epithelial morphogenesis. *bioRxiv*. 454117. doi:10.1038/s41467-023-35881-x.

Finegan, T.M., and D.T. Bergstralh. 2019. Division orientation: disentangling shape and mechanical forces. *Cell Cycle*. 18:1187–1198. doi:10.1080/15384101.2019.1617006.

Gallini, S., M. Carminati, F. De Mattia, I.A. Asteriti, and G. Guarguaglini. 2016. NuMA Phosphorylation by Aurora-A Orchestrates Spindle Orientation. *Curr. Biol.* 26:458–469. doi:10.1016/j.cub.2015.12.051.

Goldfarb, D.S., A.H. Corbett, D.A. Mason, M.T. Harreman, and S.A. Adam. 2004. Importin α: A multipurpose nuclear-transport receptor. *Trends Cell Biol.* 14:505–514.

doi:10.1016/j.tcb.2004.07.016.

Guan, X., and C.A. Fierke. 2011. Understanding protein palmitoylation: Biological significance and enzymology. *Sci. China Chem.* 54:1888–1897. doi:10.1007/s11426-011-4428-2.

Guo, L., K.S. Mohd, H. Ren, G. Xin, Q. Jiang, P.R. Clarke, and C. Zhang. 2019. Phosphorylation of importin-α1 by CDK1-cyclin B1 controls mitotic spindle assembly. *J. Cell Sci.* 132. doi:10.1242/jcs.232314.

He, S., J.P. Gillies, J.L. Zang, C.M. Córdoba-Beldad, I. Yamamoto, Y. Fujiwara, J. Grantham, M.E. DeSantis, and H. Shibuya. 2023. Distinct dynein complexes defined by DYNLRB1 and DYNLRB2 regulate mitotic and male meiotic spindle bipolarity. *Nat. Commun.* 14:1–15. doi:10.1038/s41467-023-37370-7.

Higgins, C.D., and B. Goldstein. 2010. Asymmetric cell division: A new way to divide unequally. *Curr. Biol.* 23:R1029–R1031. doi:10.1016/j.earlhumdev.2006.05.022.

Kalab, P., and R. Heald. 2008. The RanGTP gradient - A GPS for the mitotic spindle. *J. Cell Sci.* 121:1577–1586. doi:10.1242/jcs.005959.

Kaláb, P., A. Pralle, E.Y. Isacoff, R. Heald, and K. Weis. 2006. Analysis of a RanGTP-regulated gradient in mitotic somatic cells. *Nature*. 440:697–701. doi:10.1038/nature04589.

Kennedy, A.E., and A.J. Dickinson. 2014. Quantification of orofacial phenotypes in xenopus. *J. Vis. Exp.* 1–14. doi:10.3791/52062.

Kiyomitsu, T., and S. Boerner. 2021. The Nuclear Mitotic Apparatus (NuMA) Protein: A Key Player for Nuclear Formation, Spindle Assembly, and Spindle Positioning. *Front. Cell Dev. Biol.* 9:1–12. doi:10.3389/fcell.2021.653801.

Kiyomitsu, T., and I.M. Cheeseman. 2012. Chromosome-and spindle-pole-derived signals generate an intrinsic code for spindle position and orientation. *Nat. Cell Biol.* 14:311–317.

doi:10.1038/ncb2440.

Kiyomitsu, T., and I.M. Cheeseman. 2013. XCortical dynein and asymmetric membrane elongation coordinately position the spindle in anaphase. *Cell*. 154:391. doi:10.1016/j.cell.2013.06.010.

Konno, D., G. Shioi, A. Shitamukai, A. Mori, H. Kiyonari, T. Miyata, and F. Matsuzaki. 2008. Neuroepithelial progenitors undergo LGN-dependent planar divisions to maintain self-renewability during mammalian neurogenesis. *Nat. Cell Biol.* 10:93–101. doi:10.1038/ncb1673.

Kotak, S., C. Busso, and P. Gönczy. 2014. NuMA interacts with phosphoinositides and links the mitotic spindle with the plasma membrane. *EMBO J.* 33:1815–1830. doi:10.15252/embj.201488147.

Kotak, S., and P. Gönczy. 2013. Mechanisms of spindle positioning: Cortical force generators in the limelight. *Curr. Opin. Cell Biol.* 25:741–748. doi:10.1016/j.ceb.2013.07.008.

Lasser, M., B. Pratt, C. Monahan, S.W. Kim, and L.A. Lowery. 2019. The many faces of Xenopus: Xenopus laevisas a model system to study Wolf-Hirschhorn syndrome. *Front. Physiol.* 10:1–12. doi:10.3389/fphys.2019.00817.

Lin, D.T.S., and E. Conibear. 2015. ABHD17 proteins are novel protein depalmitoylases that regulate N-Ras palmitate turnover and subcellular localization. *Elife*. 4:1–14. doi:10.7554/eLife.11306.

Mariscal, J., T. Vagner, M. Kim, B. Zhou, A. Chin, M. Zandian, M.R. Freeman, S. You, A. Zijlstra, W. Yang, and D. Di Vizio. 2020. Comprehensive palmitoyl-proteomic analysis identifies distinct protein signatures for large and small cancer-derived extracellular vesicles. *J. Extracell. Vesicles*. 9. doi:10.1080/20013078.2020.1764192.

1110 Moody, S.A. 1987a. Fates of the blastomeres of the 16-cell stage Xenopus embryo. *Dev. Biol.*
1111 119:560–578. doi:10.1016/0012-1606(87)90059-5.
1112 Moody, S.A. 1987b. Fates of the blastomeres of the 32-cell-stage Xenopus embryo. *Dev. Biol.*
1113 122:300–319. doi:10.1016/0012-1606(87)90296-X.
1114 Neville, K.E., T.M. Finegan, N. Lowe, P.M. Bellomio, D. Na, and D.T. Bergstralh. 2022. The
1115 Drosophila mitotic spindle orientation machinery requires activation, not just localization.
1116 *bioRxiv*.
1117 Ning, W., P. Jiang, Y. Guo, C. Wang, X. Tan, W. Zhang, D. Peng, and Y. Xue. 2021. GPS-Palm:
1118 A deep learning-based graphic presentation system for the prediction of S-palmitoylation
1119 sites in proteins. *Brief. Bioinform.* 22:1836–1847. doi:10.1093/bib/bbaa038.
1120 Oka, M., and Y. Yoneda. 2018. Importin α: Functions as a nuclear transport factor and beyond.
1121 *Proc. Japan Acad. Ser. B Phys. Biol. Sci.* 94:259–274. doi:10.2183/pjab.94.018.
1122 Okumura, M., T. Natsume, M.T. Kanemaki, and T. Kiyomitsu. 2018. Dynein–dynactin–NuMA
1123 clusters generate cortical spindle-pulling forces as a multiarm ensemble. *Elife*. 7:1–24.
1124 doi:10.7554/eLife.36559.
1125 Ozugergin, I., and A. Piekny. 2021. Complementary functions for the Ran gradient during
1126 division. *Small GTPases*. 12:177–187. doi:10.1080/21541248.2020.1725371.
1127 Pietro, F., A. Echard, and X. Morin. 2016. Regulation of mitotic spindle orientation: an
1128 integrated view. *EMBO Rep.* 17:1106–1130. doi:10.15252/embr.201642292.
1129 Pirovano, L., S. Culurgioni, M. Carminati, A. Alfieri, S. Monzani, V. Cecatiello, C. Gaddoni, F.
1130 Rizzelli, J. Foadi, S. Pasqualato, and M. Mapelli. 2019. Hexameric NuMA:LGN structures
1131 promote multivalent interactions required for planar epithelial divisions. *Nat. Commun.* 10.
1132 doi:10.1038/s41467-019-09999-w.

1133 Proffitt, K.D., B. Madan, Z. Ke, V. Pendharkar, L. Ding, M.A. Lee, R.N. Hannoush, and D.M.
1134 Virshup. 2013. Pharmacological inhibition of the Wnt acyltransferase PORCN prevents
1135 growth of WNT-driven mammary cancer. *Cancer Res.* 73:502–507. doi:10.1158/0008-
1136 5472.CAN-12-2258.
1137 Razuvaeva, A. V., L. Graziadio, V. Palumbo, G.A. Pavlova, J. V. Popova, A. V. Pindyurin, S.
1138 Bonaccorsi, M.P. Somma, and M. Gatti. 2023. The Multiple Mitotic Roles of the ASPM
1139 Orthologous Proteins: Insight into the Etiology of ASPM-Dependent Microcephaly. *Cells*.
1140 12:922. doi:10.3390/cells12060922.
1141 Saadaoui, M., M. Machicoane, F. di Pietro, F. Etoc, A. Echard, and X. Morin. 2014. Dlg1
1142 controls planar spindle orientation in the neuroepithelium through direct interaction with
1143 LGN. *J. Cell Biol.* 206:707–717. doi:10.1083/jcb.201405060.
1144 Schelar, E. and, and J. Liu. 2008. 基因的改变NIH Public Access. *Bone*. 23:1–7.
1145 doi:10.1038/nmeth.1293.Large-Scale.
1146 Schiller, E.A., and D.T. Bergstralh. 2021. Interaction between Discs large and
1147 Pins/LGN/GPSM2: a comparison across species. *Biol. Open*. 10:1–10.
1148 doi:10.1242/bio.058982.
1149 Seldin, L., N.D. Poulson, H.P. Foote, and T. Lechler. 2013. NuMA localization, stability, and
1150 function in spindle orientation involve 4.1 and Cdk1 interactions. *Mol. Biol. Cell*. 24:3651–
1151 3662. doi:10.1091/mbc.E13-05-0277.
1152 Serwa, R.A., F. Abaitua, E. Krause, E.W. Tate, and P. O'Hare. 2015. Systems Analysis of
1153 Protein Fatty Acylation in Herpes Simplex Virus-Infected Cells Using Chemical
1154 Proteomics. *Chem. Biol.* 22:1008–1017. doi:10.1016/j.chembiol.2015.06.024.
1155 Shantanam, S., and MUELLER. 2018. Modeling human craniofacial disorders in Xenopus.

Physiol. Behav. 176:139–148. doi:10.1007/s40139-017-0128-8.Modeling.

Singh, D., N. Schmidt, F. Müller, T. Bange, and A.W. Bird. 2021. Destabilization of Long Astral Microtubules via Cdk1-Dependent Removal of GTSE1 from Their Plus Ends Facilitates Prometaphase Spindle Orientation. *Curr. Biol.* 31:766-781.e8. doi:10.1016/j.cub.2020.11.040.

Sobocinska, J., P. Roszczenko-Jasinska, M. Zareba-Kozio, A. Hromada-Judycka, O. V. Matveichuk, G. Traczyk, K. Ukasiuk, and K. Kwiatkowska. 2018. Lipopolysaccharide Upregulates Palmitoylated Enzymes of the Phosphatidylinositol Cycle: An Insight from Proteomic Studies. *Mol. Cell. Proteomics*. 17:233–254. doi:10.1074/mcp.RA117.000050.

Soderholm, J.F., S.L. Bird, P. Kalab, Y. Sampathkumar, K. Hasegawa, M. Uehara-Bingen, K. Weis, and R. Heald. 2011. Importazole, a small molecule inhibitor of the transport receptor importin-β. *ACS Chem Biol*. 6:700–708. doi:10.1016/j.earlhumdev.2006.05.022.

Stooke-Vaughan, G.A., L.A. Davidson, and S. Woolner. 2017. Xenopus as a model for studies in mechanical stress and cell division. *Genesis*. 55. doi:10.1002/dvg.23004.

Suzuki, S., J. Namiki, S. Shibata, Y. Mastuzaki, and H. Okano. 2010. The neural stem/progenitor cell marker nestin is expressed in proliferative endothelial cells, but not in mature vasculature. *J. Histochem. Cytochem.* 58:721–730. doi:10.1369/jhc.2010.955609.

Takeda, E., T. Murakami, G. Matsuda, H. Murakami, T. Zako, M. Maeda, and Y. Aida. 2011. Nuclear exportin receptor cas regulates the NPI-1-mediated nuclear import of HIV-1 vpr. *PLoS One*. 6. doi:10.1371/journal.pone.0027815.

Tamanoi, F., C.L. Gau, C. Jiang, H. Edamatsu, and J. Kato-Stankiewicz. 2001. Protein farnesylation in mammalian cells: Effects of farnesyltransferase inhibitors on cancer cells. *Cell. Mol. Life Sci.* 58:1636–1649. doi:10.1007/PL00000802.

1179 Tang, X., J.J. Punch, and W.L. Lee. 2009. A CAAX motif can compensate for the PH domain of
1180 Num1 for cortical dynein attachment. *Cell Cycle*. 8:3182–3190. doi:10.4161/cc.8.19.9731.
1181 Tarannum, N., R. Singh, and S. Woolner. 2022. Sculpting an Embryo: The Interplay between
1182 Mechanical Force and Cell Division. *J. Dev. Biol.* 10. doi:10.3390/jdb10030037.
1183 Taverna, E., M. Götz, and W.B. Huttner. 2014. The cell biology of neurogenesis: toward an
1184 understanding of the development and evolution of the neocortex. 30. 465–502 pp.
1185 Thinon, E., J.P. Fernandez, H. Molina, and H.C. Hang. 2018. Selective Enrichment and Direct
1186 Analysis of Protein S-Palmitoylation Sites. *J. Proteome Res.* 17:1907–1922.
1187 doi:10.1021/acs.jproteome.8b00002.
1188 Thomas, P.D., D. Ebert, A. Muruganujan, T. Mushayahama, L.P. Albou, and H. Mi. 2022.
1189 PANTHER: Making genome-scale phylogenetics accessible to all. *Protein Sci.* 31:8–22.
1190 doi:10.1002/pro.4218.
1191 Toyoshima, F., and E. Nishida. 2007. Integrin-mediated adhesion orients the spindle parallel to
1192 the substratum in an EB1- and myosin X-dependent manner. *EMBO J.* 26:1487–1498.
1193 doi:10.1038/sj.emboj.7601599.
1194 Tsuchiya, K., H. Hayashi, M. Nishina, M. Okumura, Y. Sato, M.T. Kanemaki, G. Goshima, and
1195 T. Kiyomitsu. 2021. Ran-GTP Is Non-essential to Activate NuMA for Mitotic Spindle-Pole
1196 Focusing but Dynamically Polarizes HURP Near Chromosomes. *Curr. Biol.* 31:115-127.e3.
1197 doi:10.1016/j.cub.2020.09.091.
1198 Wagstaff, K.M., H. Sivakumaran, S.M. Heaton, D. Harrich, and D.A. Jans. 2012. Ivermectin is a
1199 specific inhibitor of importin α/β-mediated nuclear import able to inhibit replication of
1200 HIV-1 and dengue virus. *Biochem. J.* 443:851–856. doi:10.1042/BJ20120150.
1201 Weaver, L.N., and C.E. Walczak. 2015. Spatial gradients controlling spindle assembly. *Biochem.*

Soc. Trans. 43:7–12. doi:10.1042/BST20140243.

Won, S.J., and B.R. Martin. 2018. Temporal Profiling Establishes a Dynamic S-Palmitoylation Cycle. *ACS Chem. Biol.* 13:1560–1568. doi:10.1021/acschembio.8b00157.

Yang, Y., M. Liu, D. Li, J. Ran, J. Gao, S. Suo, S. Sun-Cong, and J. Zhou. 2014. CYLD regulates spindle orientation by stabilizing astral microtubules and promoting dishevelled-NuMA-dynein/ dynactin complex formation. *Proc. Natl. Acad. Sci. U. S. A.* 111:2158–2163. doi:10.1073/pnas.1319341111.

Yu, F., X. Morin, Y. Cai, X. Yang, and W. Chia. 2000. Analysis of partner of inscuteable, a novel player of Drosophila asymmetric divisions, reveals two distinct steps in inscuteable apical localization. *Cell.* 100:399–409. doi:10.1016/S0092-8674(00)80676-5.

Yu, M., K. Qin, J. Fan, G. Zhao, P. Zhao, W. Zeng, C. Chen, A. Wang, Y. Wang, J. Zhong, Y. Zhu, W. Wagstaff, R.C. Haydon, H.H. Luu, S. Ho, M.J. Lee, J. Strelzow, R.R. Reid, and T.C. He. 2024. The evolving roles of Wnt signaling in stem cell proliferation and differentiation, the development of human diseases, and therapeutic opportunities. *Genes Dis.* 11:101026. doi:10.1016/j.gendis.2023.04.042.

Zheng, Z., Q. Wan, J. Liu, H. Zhu, X. Chu, and Q. Du. 2013. Evidence for dynein and astral microtubule-mediated cortical release and transport of Gαi/LGN/NuMA complex in mitotic cells. *Mol. Biol. Cell.* 24:901–913. doi:10.1091/mbc.E12-06-0458.

Zhong, T., X. Gongye, M. Wang, and J. Yu. 2022. Understanding the underlying mechanisms governing spindle orientation : How far are we from there ? 1–7. doi:10.1111/jcmm.17526.

Zhou, B., Y. Wang, Y. Yan, J. Mariscal, D. Di Vizio, M.R. Freeman, and W. Yang. 2019. Low-background acyl-biotinyl exchange largely eliminates the coisolation of non- s-acylated proteins and enables deep s-acylproteomic analysis. *Anal. Chem.* 91:9858–9866.

doi:10.1021/acs.analchem.9b01520.

Zhou, C.Y., B. Dekker, Z. Liu, H. Cabrera, J. Ryan, J. Dekker, and R. Heald. 2023. Mitotic chromosomes scale to nuclear-cytoplasmic ratio and cell size in xenopus. *Elife*. 12. doi:10.7554/eLife.84360.